

VĚDECKÉ SPISY VYSOKÉHO UČENÍ TECHNICKÉHO V BRNĚ

Edice PhD Thesis, sv. 868

ISSN 1213-4198

thesis
?
IS

Ing. Petr Lepcio

**Effect of Sub-Micrometer
Structural Features
on Rheology of Polymer Nanocomposites**



CENTRAL EUROPEAN INSTITUTE OF TECHNOLOGY

STŘEDOEVROPSKÝ TECHNOLOGICKÝ INSTITUT

**EFFECT OF SUB-MICROMETER STRUCTURAL FEATURES
ON RHEOLOGY OF POLYMER NANOCOMPOSITES**

**EFEKT SUBMIKROMETRICKÝCH RYSŮ NA REOLOGII POLYMERNÍCH
NANOKOMPOZITŮ**

ZKRÁCENÁ VERZE PH.D. THESIS

OBOR	Pokročilé materiály
AUTOR PRÁCE	Ing. Petr Lepcio
ŠKOLITEL	prof. RNDr. Josef Jančář, CSc.
OPONENTI	prof. Ing. Ivan Chodák, DrSc. doc. Ing. Marián Lehocký, Ph.D.
DATUM OBHAJOBY	11. prosince 2018

Brno 2018

Keywords:

Polymer nanocomposite (PNC), nanoparticle (NP), structure, spatial organization, dispersion, aggregate, chain bound cluster, depletion attraction, adsorption, acid-base interaction, solution blending, rheology, large amplitude oscillatory shear (LAOS), transmission electron microscopy (TEM), ultra-small angle X-ray scattering (USAXS), polystyrene (PS), poly(methyl methacrylate) (PMMA), silica, polyhedral oligomeric silsesquioxane (POSS)

Klíčová slova:

Polymerní nanokompozit, nanočástice, struktura, prostorové uspořádání, disperze, agregát, klastr, atrakce ve vypuzeném objemu, adsorpce, acidobazická interakce, roztokové míchání, rheologie, oscilační smyk s vysokou amplitudou (LAOS), transmisní elektronová mikroskopie (TEM), rentgenový rozptyl v ultra-malých úhlech (USAXS), polystyrene (PS), poly(methyl methakrylát) (PMMA), silika, polyhedrální oligomerní silsesquioxan (POSS)

MÍSTO ULOŽENÍ PRÁCE

Originál dizertační práce je uložen na Studijním oddělení Středoevropského technologického institutu Vysokého učení technického v Brně.

DECLARATION

I declare that the thesis has been composed entirely by myself and that all the quotations of the literary sources are accurate and complete. The presented results are the property of the Central European Institute of Technology of the Brno University of Technology and all commercial uses are allowed only if approved by both the supervisor and the director of the Central European Institute, BUT. The thesis includes copyrighted content which further use may require a permission from the copyright owner.

© Petr Lepcio, 2018

ISBN 978-80-214-5703-4

ISSN 1213-4198

1. Content

1.	Content	3
2.	Introduction	5
3.	State of the art	6
3.1.	Self-assembled polymer nanocomposites	7
3.2.	Rheological properties of polymer nanocomposites	10
3.2.1.	Steady-flow rheology	10
4.	Aims of thesis.....	10
5.	Methods.....	11
6.	Results and discussion.....	13
6.1.	Silica in poly(methyl methacrylate)	13
6.2.	Silica in polystyrene	23
7.	Conclusions	25
8.	References	26
9.	Author's CV	29
10.	Abstract	30

2. Introduction

Synthetic and natural polymers and composites are being increasingly utilized in fields ranging from aerospace to tissue engineering. A considerable scientific effort has recently focused on the enhancement of thermomechanical, optical, electromagnetic, and barrier properties of polymers by adding nanoparticles (NPs). The resulting material is usually referred to as a polymer nanocomposite (PNC), i.e., a composite with polymer matrix and one or more *nano*-structured components ($\lesssim 100$ nm). The essential advantage of nanofillers is their large surface area which amplifies the surface effects which is responsible for the property enhancement. Wide range of properties could be modified by the introduction of relatively small amount of nanoparticles into a polymer matrix, and, thus PNCs can achieve properties comparable or even superior to conventional composites at extraordinary low filler loadings.

Polymer nanocomposites represent a promising and progressive field which could meet the recent challenges of the material development. Despite the unceasing progress in the development of conventional materials such as metals and ceramics, many scientists believe that the future of material engineering lies in novel *bottom-up* platforms for additive manufacturing. Besides their *eco-friendliness* and the capability to fabricate materials with advanced *physico-chemical* properties, these techniques can keep the processing relatively simple and highly customizable by adding *end-use specific* functions while minimizing the number of the required components. The only principal limitation of the *bottom-up* methods is the size of the primary building block which is used to build up larger objects. The elementary building blocks of PNCs are represented by polymer matrix and nanoparticles. If assembled in a specific geometrical manner, it allows for a synergistic gain in properties. Since any given property requires a specific NP organization, no single length scale NP spatial organization can optimize all macroscopic properties simultaneously. Hierarchical systems, on the other hand, could be adjusted to optimize processes and properties which originate at various length scales as it is often observed in natural materials like wood,^{1,2} bone³⁻⁵ or nacre,^{4,6} which combine properties that are typically contradictory in artificial materials, such as a high stiffness and a high toughness. The tiny size of nanoparticles enables a fine tuning of the structure in several hierarchical levels when the assemblies become the building blocks of the next step. This way, the material is precisely built up from the *nano*- to the *macro*-scale with a complex structure over the whole length scale. However, despite the near perfection of the natural processes, the industrial application longs for a technique that would fabricate parts quicker than by the rate of a growing tree.

The spatial organization adjustment at the *nano*-scale has to solve the following limitations: (i) there is limited to no ability to manipulate nanoobjects directly and exclusively, (ii) mutual positions available to nanoobjects are severely constrained by thermodynamic potentials, and (iii) some thermodynamically stable structures could be kinetically inaccessible due to the presence of energetic wells and barriers unless an adequate preparation protocol is adopted. Hence, the NP spatial organization in an amorphous polymer results from a complicated interplay between the thermodynamically controlled NP organization in the liquid phase, mixing kinetics in the liquid nanocomposite and the kinetics of the liquid nanocomposite vitrification. While significant progress has recently been made in the development of theories for predicting the equilibrium structure of the PNCs, there is a strong need to address the effects of processing and kinetic entrapment on the development of their structure.

In liquid polymer, NPs can assemble in three limiting structures – NP agglomerates, chain bound NP clusters or individually dispersed NPs⁷. At this point, the meaning of “aggregate” and “agglomerate” should be clarified since a widespread confusion exists with different authors and fields preferring various nomenclatures. The terms are often freely interchanged and the only mutual agreement is that both are related to assemblies of primary particles⁸. This work considers

convenient to distinguish between these two terms; therefore, aggregate will be used for an arrangement of rigidly adjoining particles while agglomerate will mark a much looser and weaker assemblage, such as a flocculate. The distinguishing criteria is whether the particles can or cannot undergo a spontaneous rearrangement due to the thermal motion. NPs in aggregate interact directly with each other and the NP-NP attraction prevails all the interfacial interactions in the system. In the case of the chain bound clusters, particles are separated by polymer chains which mediate the NP-NP interaction while a single “*bridging*” chain adsorbs on multiple particles. Therefore, NP clusters behave as internally structured inclusions. Dispersion of individual NPs maximizes the NP-chain interfacial area per unit volume which results in the greatest extent of polymer affected by the particles. Segments of adsorbing chains are immobilized on the particle surface and frustrate the packing in their vicinity which is reflected in macroscopic deformation response. However, the course of the NP spatial organization through the transition between the equilibrium PNC liquid and the solid-state bulk material has not been fully understood yet. Answering the related questions might also boost other fields not typically considered as nanocomposites, e.g. additives and stabilizers for plastics. Meanwhile, the incomplete theoretical understanding did not stop PNCs to enter the worldwide market. Besides car tires which utilize carbon black reinforced rubber for decades, the range of nanocomposite components in automotive has been growing ever since its first application as step assists in 2002⁹.

The thesis reports on solution blending preparation protocols and the outcoming NP spatial organizations in a glass forming polymer. The structure control was achieved by changing the processing conditions, yielding either dispersed, agglomerated or clustered NPs which were fixed by the rapid solvent evaporation and remained kinetically stable through the consequent excessive thermal processing. The qualitative differences between the structural types manifested by their properties and formation kinetics were emphasized. Two types of aggregates were recognized, one of a kinetical and one of a thermodynamic origin, both dissimilar to what was identified as the chain bound clusters which supposedly emerged from a solvent mediated analogue of bridging predicted by the PRISM theory of Schweizer et al⁷. The structural information of the *submicro*-shaped PNC features was combined with their rheological behavior to provide novel experimental evidence on the NP ordering in model PNC systems.

3. State of the art

The field of particle dispersion in polymer nanocomposites can benefit from some well-established concepts of colloidal chemistry such as colloidal hard and soft spheres, DLVO theory, etc. Colloidal particles generally tend to stick closely together due to the attractive van der Waals forces unless their dispersion is stabilized by other forces. When considering nanoparticles, theoretical models should incorporate the NP atomic-scale surface patchiness to encompass the distribution of interaction potential between the nanoparticle surface and neighboring bodies¹⁰. However, the complex situation is often simplified by the 12-6 power law also known as the Lennard-Jones potential¹¹. In the case of charged particles, the Coulomb repulsion can act as the stabilizing force as described by the DLVO theory. Moreover, hydrophilic repulsion and hydrophobic attraction may arise next to the electrostatic double layer and van der Waals interactions as additional forces between the hydrophobic and hydrophilic surfaces. This case is, however, beyond the scope of the DLVO model¹². Steric repulsion is another stabilization effect and will be discussed in greater detail further in the text since it is particularly relevant to the PNCs. Other interactions can be induced in PNCs if the system is subjected to an external electric, magnetic or shear force field.

Particles can be either randomly dispersed in space or arranged in a regular pattern. Higher maximum concentration could be achieved in the latter case than in the former¹³. For monodisperse spheres in close packing, the theoretical maximum is ~ 0.74 but higher values can be achieved for

polydisperse or non-spherical particles. If dense packing of particles is favored, polyhedral specks incline to maximize their face-to-face contact, non-spherical smoothly shaped particles prefer contact at sites with lower principal curvature and non-centrosymmetric particles can exploit their rotational degrees of freedom¹⁴. In a polymer matrix, NPs can occupy one of the three basic spatial organizations – aggregated, clustered and dispersed NPs. Particles in aggregates lie in (near) contact with each other and the whole aggregate resembles one large particle. Despite the aggregated particles do not fuse together to yield a new particle with reduced surface like in the case of coalescence, some surface sites may be blocked¹¹ and the effective surface area – the surface available for interaction with polymer chains – is reduced.

Clusters are built up from particles bridged by adsorbed polymer chains, which mediate the interparticle interactions. They also seem to act as one independent entity but, unlike aggregates, clusters are principally two-level hierarchical systems where the higher level is represented by stiff inclusions in polymer matrix while the lower level encompasses both the NPs and the polymer chains. Finally, good dispersion of individual particles ensures that the whole NP surface is exposed to the polymer and the amount of affected matrix is maximized. Consequently, good dispersion usually exhibits the most pronounced change in properties^{15–17} and is particularly favored in fundamental studies and optical applications. The structural impact on PNC material properties is described in the following chapter. Despite the enormous effort and the huge amount of published papers^{15,16,18–36}, a reliable prediction of experimentally prepared dispersion states has not yet been fully achieved and the “*trial-error*” approach still dominates many of the studies on the NP spatial organization in PNCs. It is not unanimously agreed which physical parameters govern the formation and properties of self-assembled nanoparticle-polymer structures.

3.1. Self-assembled polymer nanocomposites

Steric stabilization is induced by polymer chains attached to NP surface, either by the covalent bond or by the less permanent physical interaction, since the polymer shells repel each other on approach due to the gradually increasing entropic penalty of distorting chains. If the polymer chains are not permanently attached to the particle surface by covalent bond, the enthalpy of chain adsorption onto the particle needs to be considered.

The coil dimension of an adsorbed chain can shrink, expand or retain its original size relative to the chains in bulk^{37,38} and a theory on substantial conformational changes upon chain adsorption onto NP surface was proposed²⁸. NMR experiments for silica-polyethylene glycol (PEG) nanocomposite revealed that the adsorbed polymer consists of segments with three degrees of mobility³⁹. Closest to the NP surface, 1–2 segments in the direct contact form a rigid glassy layer which fraction is independent of the molecular weight and, for a given NP size, it scales accordingly with the particle concentration. Mobile segments distant more than one radius of gyration from the surface are, on the other hand, are not influenced by NPs and relax alike to the chains in the bulk polymer. Finally, there is a fraction of segments, presumably tails and loops in proximity to NP surface³⁹, which are partially constrained, and their relaxation times take values intermediate to the two previous cases.

Mackay, et al.²⁸ appointed the governing role to a sole parameter represented by the particle radius to polymer gyration radius ratio. They proposed a qualitative model that good dispersion is obtained only when the particle radius is smaller than the polymer radius of gyration (Fig. 1A). Hooper and Schweizer^{7,40–42} applied the microscopic polymer reference interaction site model (PRISM) to predict the dispersion and the interparticle potential of mean force (PMF) for hard spheres in adsorbing homopolymer melt (Fig. 1B). Their model predicts an unfavorable chain adsorption onto particles at low polymer-NP interfacial energy and a contact aggregation induced by the consequent entropically-driven depletion attraction between the particles as the polymer chains keep off the NP

surface. The amplitude of the depletion force is proportional to the particle size and results in strong attraction even in the case of particles as small as 10 nm⁴⁰. When the particle-chain interaction strengthens, the prospect of the polymer adsorption onto the particle increases and results into the dispersed sterically-stabilized state⁷. The enthalpic gain of the polymer adsorption gradually rises in importance upon the increasing polymer-NP interfacial strength until it eventually takes over and dominates the system while the dispersed structure is obtained. Hence, the transition from the dispersed to the aggregated state at low interfacial energies was identified as an enthalpically-driven phase separation.

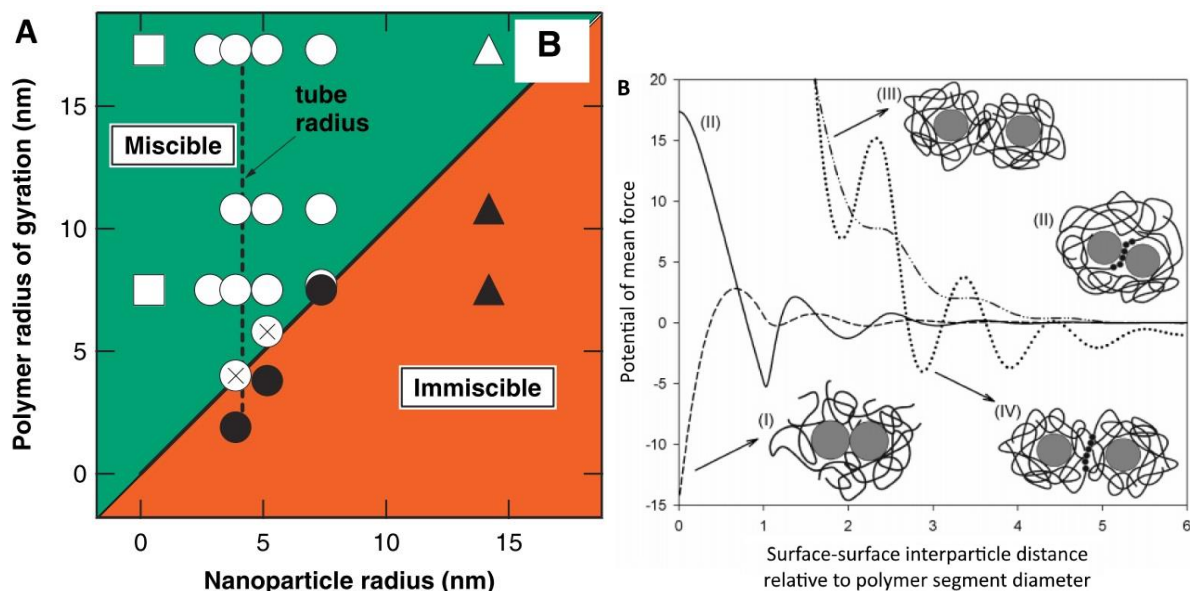


Fig. 1: (A) Phase diagram of polymer nanocomposites. Solid symbols represent the phase separated systems while open symbols stand for the miscible ones. The cases with agglomeration detected by SANS but without large-scale phase separation are marked by open circles with a cross. Squares denote C₆₀/PS nanocomposites, circles PS NPs/PS matrix nanocomposites, and triangles the dendritic PE/PS system. The filler content was 2 wt.% for all the presented data. Reprinted with a permission from the ref.²⁸. Copyright 2006 Science. (B) Particle-particle potential of mean force dependence on the interparticle distance relative to the polymer segment diameter according to the PRISM theory for representative examples of **I.** contact aggregation, **II.** bridging, **III.** dispersed state (steric stabilization), **IV.** telebridging. Reprinted with a permission from the ref.⁷. Copyright 2006 American Chemical Society.

For even stronger particle-chain attraction, a polymer induced NP bridging state emerges as a consequence of strongly adsorbed polymer layers onto the NPs. The corresponding enthalpic gain of the adsorption overwhelms the entropic loss of the chain conformational change connected with the polymer adsorption and the steric repulsion diminishes. Once already distorted, segments of this chain will preferentially adsorb onto another particle rather than a chain which has not paid the entropic penalty, yet. As a result, particles become bridged by polymer chains into clusters. In the clusters, the average interparticle separation of the nearest neighbors corresponds to one monomer diameter⁷. Therefore, the phase separation at strong NP-chain interaction is enthalpically dominated. Finally, *telebridging* is similar to bridging but occurs at longer interparticle distances when the spatial reach of the polymer-particle interaction favors presence of multiple layers of adsorbed chains between the bridged particles⁷. Some of the modelled PMF contains multiple energy wells (Fig. 1B) which suggests that, for certain combination of parameters, the kinetic entrapment might give rise to thermodynamically metastable structures.

Hooper and Schweizer transformed their results into phase diagrams constructed for various cases of the above-mentioned parameters. The NP-chain interaction strength ϵ_{pc} and the particle volume

fraction were the structural variables. A representative example is displayed in Fig. 2A showing that the miscibility region at medium NP-chain attraction narrows with increasing particle volume fraction⁴². The PRISM theory was successfully adopted by Zukoski, et al. to determine NP-polymer interaction strength by correlating experimental structure factors obtained from scattering measurements to the theoretical prediction^{34,36,39,43-48}. The PRISM theory fitted well to their experimental observations in the limit of low molecular weight polymers ($M_w < 1000$ for silica in polyethylene glycol) but fails for higher molecular weight polymers.

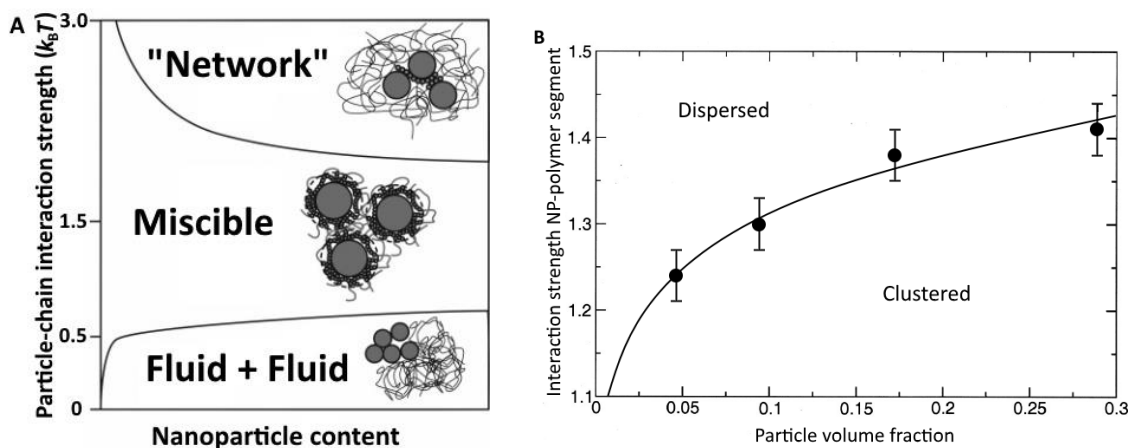


Fig. 2: Morphology diagrams of NPs in polymer matrix predicted by (A) PRISM theory (representative example). Reprinted with a permission from the ref.⁴². Copyright 2007 American Chemical Society. (B) molecular dynamics simulation. Reprinted with a permission from the ref.¹⁰. Copyright 2003 AIP Publishing.

Currently, there are several techniques for PNC fabrication but all struggle to ensure the desired dispersion of the nanofiller in the polymer matrix. The formation of the NP arrangement is typically carried out in a liquid phase since the related processes are kinetically hindered in the solid state, keeping the internal structure relatively stable over extended periods of time. Melt and solution blending are preferred and most common for thermoplastic PNCs. In general, it is difficult to obtain a good dispersion when nanoparticle powder is added to polymer melt⁵⁵⁻⁶¹. Nanoparticles are commonly aggregated in dry state and they often do not fully disperse even under extreme shear forces. Solution blending, on the other hand, allows for nanoparticle predispersion and colloidal-like solvation and stabilization effects to take place. Solvent also dilutes all interactions including the interparticle attraction³⁴, low viscosity compared to melts enhances the formation kinetics, and the solvent composition could be used as a convenient tuning parameter³³. NP-polymer assemblies occur in polymer nanocomposite solutions if the NP's affinity to polymer is superior to the affinity between the NPs and the solvent⁶². Solution blending, however, brings on a major drawback represented by the need to remove the solvent after the desired dispersion state is achieved. Evaporation rate enters the structuring phenomenon as a kinetic factor, since the post-processing of solution-casted solid-state samples does not critically impact the dispersion initially obtained after the drying³³. The solvation stabilization by electrostatic repulsion diminishes upon the solvent removal and is replaced by the kinetic stabilization due to the increasing viscosity and restricted NP diffusion; therefore, a slow evaporation rate promotes aggregation^{33,63}.

Jouault, et al.³³ provided experimental evidence for the spatial distribution of PNCs controlled by altering the effective interaction strength through the choice of solvent. Solvent molecules can either favor the polymer-depletion attraction and induce aggregation, or they can enhance the polymer adsorption and, thus, the interparticle steric repulsion resulting in a good dispersion. Zhao et al.¹⁹ proposed the relative interaction strength between the particle-solvent, and the particle-polymer as

the key forces which drive the formation of the bound polymer layer. In order to investigate solvation effects, Zukoski, et al.³⁴ tested silica-PEG nanocomposite in water and ethanol at Θ and non- Θ temperatures and concluded, that the NP dispersion is not explicitly related to the solvent quality regarding the polymer Θ state. Clearly, the role of solvent in NP assembly goes beyond its solvation impact on the dissolved polymer and is likely directly involved in the NP assembly.

3.2. Rheological properties of polymer nanocomposites

3.2.1. Steady-flow rheology

Nanocomposite melts and solutions are viewed as colloidal-size particles immersed in a liquid continuum. This concept is especially durable in the case of low molecular weight chains exhibiting Newtonian flow behavior and containing well-dispersed nanoparticles. Strongly interacting chains form an adsorbed layer around NPs while weakly interacting ones tend to slip from the NP surface and can cause a depletion attraction. As a result, the effective hydrodynamic volume of NPs is altered from that expected for bare hard spheres of the same size. Kim and Zukoski³⁶ addressed these changes by introducing an additional scaling factor k into the well-established Einstein-Stokes equation:

$$\eta_r = 1 + 2.5 k\varphi + H\varphi^2 + \dots \quad (1)$$

where η_r and φ stands for relative viscosity and particle volume fraction respectively. The value of 2.5 is the so-called Einstein's coefficient derived from the analytic solution of a flow around an isolated hard sphere. H , also sometimes marked as B_1 , is the second virial coefficient, also known as the Huggins coefficient, which reflects the interparticle interactions⁶⁴. The value of $2.5k$ equals intrinsic viscosity $[\eta]$ and could be readily assessed experimentally. Kim and Zukoski³⁶ reported values of k ranging from large positive for NPs encapsulated in strongly adsorbed polymer layers to large negative for NPs smaller than polymer radius of gyration R_G in entangled polymers³⁶. Negative intrinsic viscosity contradicts the continuum rheological models since particles distort the flow of the surrounding liquid and increase the amount of the energy distorted upon flow which is reflected in the increased viscosity⁶⁵. However, molecular dynamics simulations revealed that the NP diffusion coefficient reaches a steady value upon increasing the molecular weight of polymer medium despite it should be gradually slowed down due to the raising bulk viscosity⁶⁶. It should be noted that the equation (1) was based on experiments with fairly oligomeric chains (about 8 segments long) and does not consider other factors such as the rotation of particles which also impacts the value of the intrinsic viscosity⁶⁵. Small NPs of the size equal or smaller than the polymer tube diameter or the entanglement mesh-length were indeed reported to diffuse through the entangled polymer faster than predicted by the continuum Stokes-Einstein equation^{67,68}.

4. Aims of thesis

This Thesis aims at advancing fundamental understanding of the role of preparation protocol on the structure and properties of polymer nanocomposites. In particular, it focuses on investigation of the principle variables governing nanoparticle spatial organization in model PNCs prepared by solution blending. Effects of both kinetic and thermodynamic variables, e.g., particle size and shape, polymer molecular weight, particle-polymer interaction strength, temperature, shear stress and strain are investigated over a range of NP and polymer concentrations. Attempt is made to analyze the experimental rheological and thermomechanical data using structural information and existing microscopic models.

5. Methods

Commercial grade polymethylmethacrylate (PMMA) Plexiglas 8N (Evonik Industries AG, Germany) with $M_n = 50 \text{ kg}\cdot\text{mol}^{-1}$, $M_w/M_n = 1.9$, and $T_g = 113 \text{ }^\circ\text{C}$ (DSC, $10 \text{ K}\cdot\text{min}^{-1}$) was used as a matrix. Colloidal bare silica nanoparticles dispersed in isopropanol with the diameter of $20\pm 4 \text{ nm}$ IPA-ST (Nissan Chemicals, Japan) were used as the nanofiller under the commercial names IPA-ST. Colloidal nanosilica was ultrasonicated by an ultrasonic tip (Bandelin Sonopuls, Germany). Firstly, resonance frequency was found and then, ultrasonication was performed ($t_{\text{on}} = 0.1 \text{ s}$). Notably, the starting point for the PNC samples in PMMA was well-dispersed particles in isopropanol. Since isopropanol is weakly acidic ($\text{p}K_A = 16.5$) and miscible with all the solvents used in this research and its concentration in the samples was small, its role in the resulting NP spatial organization was neglected. Then, the desired amount of dispersed nanoparticles was added to polymer solution with the concentration of 66.7 mg of polymer per one milliliter of solvent (about $5.3 \text{ vol. } \%$) corresponding to the semi-dilute solution regime. Nanoparticle loading ranged from 0.5 to $10 \text{ vol. } \%$. Various solvents were used as the preparation protocol variable: THF, acetone, ethyl acetate, acetone-toluene 1:1 mixture (volumetric ratio), and toluene. All solvents were acquired from Lach-ner (Lach-Ner, s.r.o., Czechia) in p.a. purity grade. Polymer nanocomposite solutions were rigorously mixed at 1200 RPM by a magnetic stirrer for 1 hour. Subsequently, the mixture was rapidly vitrified in a pre-heated chamber at $140 \text{ }^\circ\text{C}$ and kept there for 24 hours. Grinded samples were further dried for 6 days in a vacuum oven at $140 \text{ }^\circ\text{C}$ and ca $10\text{--}20 \text{ kPa}$ to ensure a complete removal of solvent residues. Drying efficiency was checked by thermogravimetric analysis. Dried samples were further grinded and compression molded into 1 mm thick sheets at $190 \text{ }^\circ\text{C}$ in a hot press (Fontijne Pressess, Netherlands) at closing pressure of 300 kN . The pressure was not relieved until the samples were cooled down to laboratory temperature at a cooling rate of approximately $30 \text{ K}\cdot\text{min}^{-1}$.

Polymer coil size was determined utilizing DynaPro NanoStar dynamic light scattering device (WYATT, USA) in isopropanol and all the solvents used for sample preparation at various temperatures at concentration of $10 \text{ mg}\cdot\text{ml}^{-1}$ (about $0.84 \text{ vol. } \%$) which corresponds to the dilute regime. NP spatial organization and morphology of the PNCs was determined by transmission electron microscopy (TEM, Morgagni 268D 100 kV , FEI, Czech Republic) of ultrathin slides with uniform thickness of approximately 50 nm and by ultra-small-angle X-ray scattering (USAXS, Smartlab diffractometer, Rigaku, Japan) employing the copper rotating anode, 2×220 germanium monochromator and 2×220 germanium USAXS analyzer. USAXS patterns were analyzed by Guinier and Porod law. USAXS provides an average form and structure information of nanoparticles arrangement in polymer matrix.

TEM provides a direct view of silica nanoparticles arrangement in polymer matrix. The image analysis of TEM micrographs were performed to obtain the distribution function of interparticle separations. Images were chosen to contain minimum of 150 NPs . At first, the NP positions were recorded manually from the TEM images, since the automated particle recognition function failed to recognize single particles within the assemblies due to the insufficient contrast of the neighboring NPs' edges. Due to the approximately 50 nm thickness of the ultramicrotome sections, the electron beam interacts with several NPs on its path through the sample and blurs the particle edges as the 3D structure is being projected into the 2D plane. Particles located above each other will overlap in the TEM snapshot. Therefore, large aggregates are often smeared into objects of an indistinct inner organization. A closer inspection of these objects depends strongly on operator's intuition, which translates into a reduced accuracy of the analysis. In addition, one has to keep in mind that the interparticle separations seen in TEM images are undervalued since they are only 2D projections of the real distances. To extend the statistical population and improve the repeatability, the lengthy operator-dependent manual analysis of the TEM micrographs was replaced by an automated

computer-aided image analysis using smaller magnification (44 000×). Since the automated particle recognition function of the ImageJ software failed to recognize single nanoparticles in tight ensembles, the automated TEM image analysis treated clusters and aggregates as the elementary structural units where applicable. The element diameter was calculated by approximating the fitted element area to a circle.

Interparticle separations were computed as Euclidean distances of the centers for each pair of the NPs. It gives rise to $0.5 \cdot (n - 1)^2$ correlations where n is the number of NPs. The probability distribution of finding two NPs at a certain interparticle separation was calculated by dividing all the experimentally recorded values into 200 uniformly spaced discrete intervals approximately 4–5 nm wide. The experimentally assessed distribution of interparticle separation was compared to the probability \mathbb{P} of finding two randomly selected points in a square in a separation D equal or less than a threshold value d given by:

$$\mathbb{P}(D \leq d) = \iint_{\{x^2+y^2 \leq d^2\}} f(x)f(y)dx dy, \quad (2)$$

where x and y denotes the absolute value of the difference between the x and y -coordinates of the points respectively⁶⁹. For $x \in (0, a)$, the function f_x is given by:

$$f(x) = \frac{2}{a^2}(a - x), \quad 0 < x < a, \quad (3)$$

where a stands for the length of the square's side. The function f_y is defined the same way for $y \in (0, a)$. The outer integration was performed using a numerical method based on the Gaussian quadrature in GNU Octave software⁷⁰. A cut-off value of a , in the range of 700–800 nm, was selected for each image to provide a reasonable fit to the experimental data. This reflects the fact that the NPs near the image edges were not taken into account if they were part of a structure which larger portion supposedly lying beyond the image's edge. The apparent inter-element distance was determined as the mode, i.e., the most frequently occurring value, which was established from the maximum of the distribution function of the 5 nearest neighbors of each element. The number of neighbors was selected according to the coordination number in a 3D space which is, according to a simple cubic lattice model, equal to 4.68⁷¹.

Rheological measurements were executed using Ares-G2 rheometer (TA Instruments, Inc., USA) in continuous flow mode with concentric cylinder geometry. The pure polymer solutions exhibited Newtonian behavior at the concentration of interest, which corresponds to the initial mixing step of PNC preparation. Hence, all the presented results were collected at a single strain rate of 20 s^{-1} and relativized to viscosities of pure polymer solutions without NPs. The differences in the absolute viscosities of the nanocomposite solutions (1.7–2.9 mPa·s) were marginal compared to the substantial change of viscosity during the solvent evaporation which took place over 10 orders of magnitude (melt viscosity of pure matrix was $4.7 \cdot 10^7 \text{ Pa} \cdot \text{s}$ at $140 \text{ }^\circ\text{C}$). The diluting effect of isopropanol added with NPs was recognized as insignificant ($< 5 \%$ viscosity change for the highest NP concentration) and neglected except the samples in ethyl acetate where the effect was stronger and required a correction for the addition of pure isopropanol without NPs. Samples were stored in sealed glass bottles and measured one day after preparation unless stated otherwise. To minimize solvent evaporation, the procedure time was kept short (< 10 minutes) and the tests were carried out at $25.0 \text{ }^\circ\text{C}$. The same instrument was used to record the viscosity of pure polymer solutions at various temperatures, which was required as an input variable for DLS measurements. Glass transition temperature was determined from the maximum of loss modulus from the dynamic mechanical analysis using the RSA-G2 device (TA Instruments, Inc., USA) with a single cantilever geometry. Rectangular specimens of the typical size $30 \times 5 \times 1 \text{ mm}^3$ were cut from the molded sheets and their thermo-mechanical history was erased by preheating to $140 \text{ }^\circ\text{C}$ for 30 minutes. Temperature sweeps

were carried out immediately after preheating at deformation amplitude of 0.05 % and frequency of 1 Hz in the range from 140 to 90 °C with 1 °C step.

A series of PNCs was prepared from colloidal silica in ethyl methyl ketone (MEK-ST, supplied by Nissan Chemicals, Japan) and polystyrene (Sigma Aldrich, Germany), $M_w = 192 \text{ kg}\cdot\text{mol}^{-1}$, in tetrahydrofuran (THF), *N,N*-dimethylacetamide (DMAc), and cyclohexanone (all supplied by Lachner, Czechia, in p.a. purity grade) to test the results obtained for the PMMA based PNCs. The NP structural organization was investigated by scanning transmission electron microscopy (STEM) Lyra3 (Tescan, Czechia) and the rheological data was recorded by the same instrument and method as the PMMA samples. Worth noting, the samples in DMAc and cyclohexanone required a correction for the addition of pure ethyl methyl ketone due to their higher absolute viscosities (10.0 and 27.9 mPa·s, respectively).

6. Results and discussion

6.1. Silica in poly(methyl methacrylate)

As evidenced by the measurements, the silica pre-dispersed in isopropanol remained individually dispersed when added to THF, acetone and ethyl acetate and only small fraction of NPs (~2 mass %) formed aggregates ($d_{\text{mean}} = 230.8 \text{ nm}$) in acetone-toluene 1:1. Toluene did not stabilize the NP dispersion though, and a large-scale aggregation and a phase separation occurred. NP dispersion state in polymer liquid arises from the balance of the solvent–NP, NP–NP, solvent-polymer and NP-polymer interactions and the kinetic conditions of the preparation protocol (shear rate, time of solvent evaporation, viscosity, etc.). By varying the solvent strength, three different nanoparticle organizations were prepared in the silica/PMMA containing a constant NP loading of 1 vol. % (Fig. 3). They were identified as aggregates (Fig. 3A, E), individually dispersed NPs (Fig. 3B–C), and chain bound clusters (Fig. 3D). Mackay et al.²⁸ proposed hypothesis to quantitatively analyze the state of the NP dispersion in polymer liquids attributed the key role in determining the outgoing NP spatial arrangement to the ratio between the NP radius (R_{NP}) and the polymer radius of gyration (R_{G}). Using different solvents, the $R_{\text{NP}}/R_{\text{G}}$ ratio varies for the given combination of polymer and NP due to the R_{G} varying with the quality of the solvent. To test this hypothesis, the average PMMA coil diameter measured by dynamic light scattering (DLS) was approximately 10.5 nm for all solvents used in this study at the temperature range covering the blending step of the preparation protocol. The size variation lying within the experimental error was negligible. The coil diameter was always smaller than the NP diameter of $20 \pm 4 \text{ nm}$. According to the hypothesis of Mackay et al.²⁸, R_{NP} larger than the R_{G} should result in a poor NP dispersion and, a NP agglomeration should occur. This prediction contradicts the experimental observations presented in this work. However, Mackay et al.²⁸ investigated PNCs consisting of fullerenes in polyolefin or tightly cross-linked polystyrene nanoparticles in linear polystyrene matrix, i.e. systems with almost “no specific interfacial interactions”. Minimizing or eliminating the role of the adsorption enthalpy undoubtedly leads to the dominance of the entropic factors which in turn relate to the size⁷². Previous studies has already suggested the importance of the interaction balance between the components, i.e. particle-polymer-solvent, on the NP spatial organization^{10,33,41} but the current results show that adsorbing PNC solutions do not conform to the prediction based on the NP-polymer coil relative size.

Individually dispersed particles were observed in TEM images of PNC samples prepared from acetone (Fig. 3B) and ethyl acetate (Fig. 3C). The SAXS analysis of the acetone-prepared PNC confirmed the spatial organization consisting of individual particles dispersed in the matrix due to the flat low q region and the smoothly decreasing intermediate q region (Fig. 3F). Both methods yielded an average element diameter about 20 nm which matches well with the size of an individual NP.

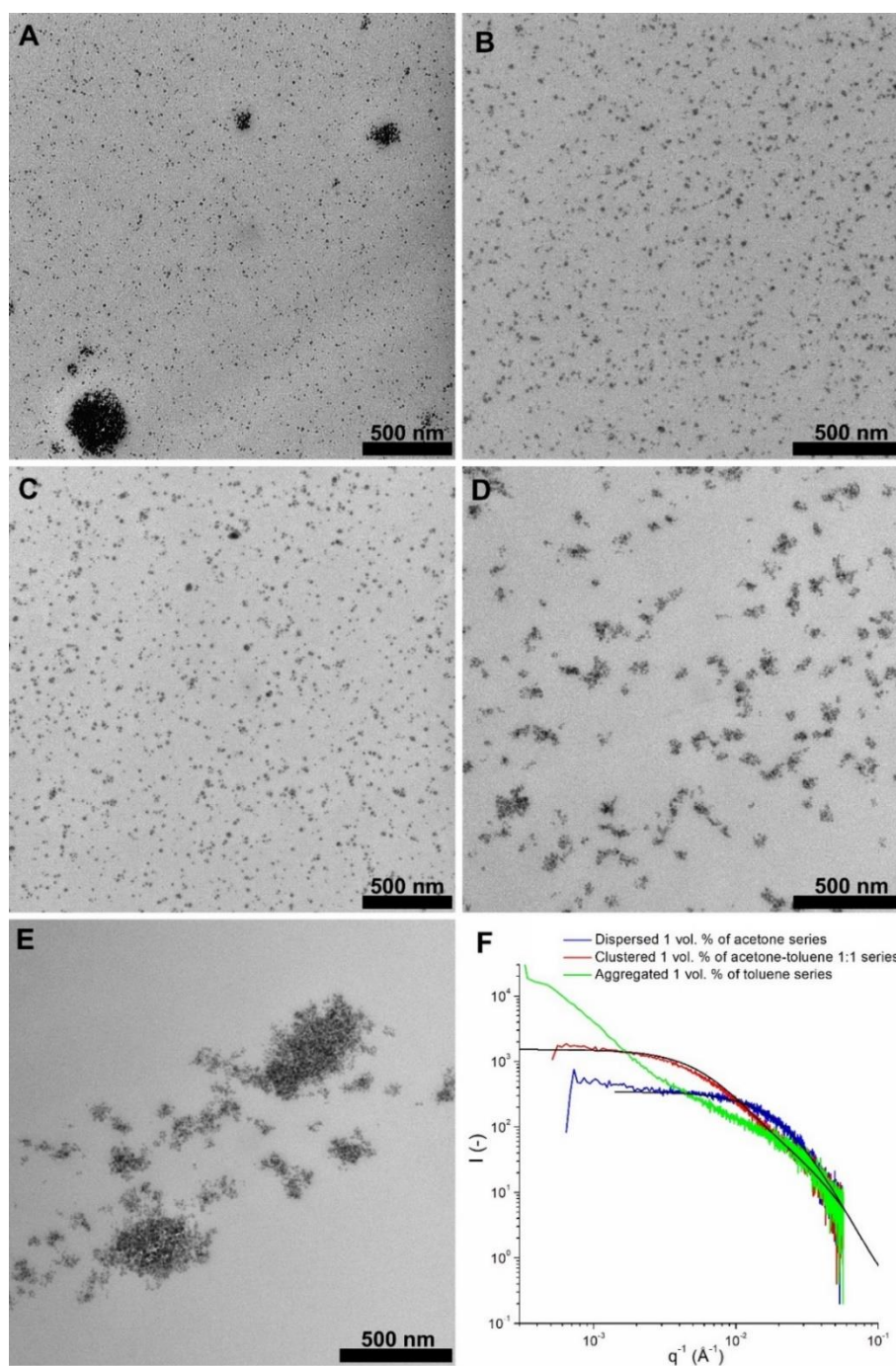


Fig. 3: TEM images (magnification 44 000 \times) of 1 vol. % PMMA/nanosilica nanocomposites with various structure prepared from (A) THF, (B) acetone, (C) ethyl acetate, (D) acetone-toluene 1:1 mixture, and (E) toluene. (F) USAXS dependence of the intensity I on the length of the scattering vector q extracted from USAXS data for PNC samples with NP loading of 1 vol. %. The black lines represent fits for dispersed and clustered nanostructures.

Chain bound clusters (Fig. 3D) were formed using the 1:1 acetone-toluene mixture solvent. Three populations of cluster sizes were found alongside less frequent single particles. The smallest clusters contained 2 to 3 particles (the least frequent occurrence), the intermediate clusters contained 5 to 9 NPs, and the large clusters consisted of 16 to 26 particles (the most frequent occurrence). Theoretical models¹⁰ suggest a gradual increase of the cluster size with time assuming that individual particles form small clusters consisting of two to three nanoparticles and once formed, these elementary

clusters connect to build up larger clusters. An evidence of gradual cluster formation was indeed observed as will be discussed later. The USAXS results showed a complex behavior in the low and the intermediate q regions (Fig. 3F), indicating the presence of two scattering populations which confirms that the PNC contained internally structured inclusions – clusters with size of ~45 nm and primary building blocks with size of 20 nm.

Finally, preparing the PNC utilizing THF (Fig. 3A) or toluene (Fig. 3E) resulted in aggregates of NPs in a close contact with the average aggregate size of approximately 400 and 500 nm, respectively. In THF, a fraction of NPs remained individually dispersed alongside the aggregates, but it will be referred to this NP organization type as “aggregated” for simplicity and to highlight the presence of the large NP ensembles. The USAXS profiles of PNC prepared from toluene also revealed a presence of big and small populations of multi-NP agglomerates of a size larger than 100 nm. However, the origin of the aggregation in THF and toluene shares little in common and derives from two very different processes as will be described below.

TEM micrographs were subjected to image analysis to provide additional information on the NP arrangement. Clearly, the solution blending in acetone favors dispersion since the experimental probability distribution of the interparticle distances conforms well to the random distribution except for very low separations. The discrepancy clearly suggests presence of small NP ensembles. However, it was beyond the limit of the instrumentation to determine whether these are chain bridged, or aggregated NPs and the decisive evidence needs to be searched elsewhere. The partial replacement of acetone by toluene as the solvent in the processing step introduces NP association. The interparticle separation distribution function reveals that the NP ensembles are on average 48.3 nm large and about 120–150 nm apart from each other. These results fairly agree with the findings of the automated image analysis which provides credibility to the automated evaluation process. The ratio of the interelement distance (Fig. 4A) to the element diameter (Fig. 4B) conformed well to the random distribution¹³ for all the evaluated samples within the whole investigated concentration range. It validates the idea that aggregates/clusters shall be regarded as sovereign entities randomly dispersed in the polymer matrix and that a balance was established between their size and the separation distance, likely during the annealing phase of the processing.

The distance parameter Ra (eq. 5) of PMMA/acetone and PMMA/acetone-toluene 1:1 mixture takes values of 6.30 and 6.69, respectively⁷³ or, for another set of solubility parameters,⁷⁴ equals to 5.50 and 5.35, respectively. In both cases, the overall interactions are nearly similar, which agrees with the expectation that the final NP dispersion is not directly tied to the quality of the solvent respective to the polymer theta condition³⁴. However, polar contribution is more favored in acetone while the dispersion contribution prevails in acetone-toluene 1:1 mixture. Obviously, the tremendous structuring impact of the solvent must be caused by another mechanism. We propose that it is the solvent interaction with NPs which governs the resulting NP spatial organization. The solubility parameter concept was originally developed in organic chemistry, and, thus, values for silica NPs are not readily available in literature. Therefore, we present procedure to estimate the value of the solubility parameters for silica. As described above, polymer is desorbed from silica surface upon addition of a co-solvent – displacer - at the critical volume fraction φ_c . Partial solubility parameters, $\delta_{part.}$, of the solvent-mixture is calculated as the average of both components weighed by the respective volume fractions:

$$\delta_{part.,mix} = \varphi_c \delta_{part.,d} + (1 - \varphi_c) \delta_{part.,s}, \quad (4)$$

where the subscripts ‘mix’, ‘d’ and ‘s’ regard to the mixture, displacer and solvent, respectively. At the critical displacer volume fraction, it is expected that the silica affinity to polymer equals its affinity to the medium (solvent-displacer mixture), therefore:

$$Ra_{(silica/polymer)}^2 = Ra_{(silica/medium)}^2, \quad (5)$$

$$4(\delta_{D,S} - \delta_{D,p})^2 + (\delta_{P,S} - \delta_{P,p})^2 + (\delta_{H,S} - \delta_{H,p})^2 = 4(\delta_{D,S} - \delta_{D,mix})^2 + (\delta_{P,S} - \delta_{P,mix})^2 + (\delta_{H,S} - \delta_{H,mix})^2, \quad (6)$$

where the subscripts ‘S’ and ‘p’ refers to silica and polymer respectively. Expanded and rearranged, the equation yields:

$$A \cdot \delta_{D,S} + B \cdot \delta_{P,S} + C \cdot \delta_{H,S} = D, \quad (7)$$

$$A = 8(\delta_{D,p} - \delta_{D,mix}); B = 2(\delta_{P,p} - \delta_{P,mix}); C = 2(\delta_{H,p} - \delta_{H,mix}), \quad (8)$$

$$D = 4\delta_{D,p}^2 - 4\delta_{D,mix}^2 + \delta_{P,p}^2 - \delta_{P,mix}^2 + \delta_{H,p}^2 - \delta_{H,mix}^2 \quad (9)$$

which is a three-variable linear equation and could be solved for three independent sets of parameters A , B , C and D . The silica dispersive ($\delta_{D,S}$), polar ($\delta_{P,S}$) and hydrogen bonding ($\delta_{H,S}$) partial solubility parameters were calculated for each combination of 3 displacers of PMMA in carbon tetrachloride out of 6 available⁷⁵ and yielded values of $(18.8 \pm 1.0) (\text{J} \cdot \text{cm}^{-3})^{0.5}$, $(5.7 \pm 0.8) (\text{J} \cdot \text{cm}^{-3})^{0.5}$ and $(6.3 \pm 0.8) (\text{J} \cdot \text{cm}^{-3})^{0.5}$, respectively (Table 2). Since the solubility parameter was originally

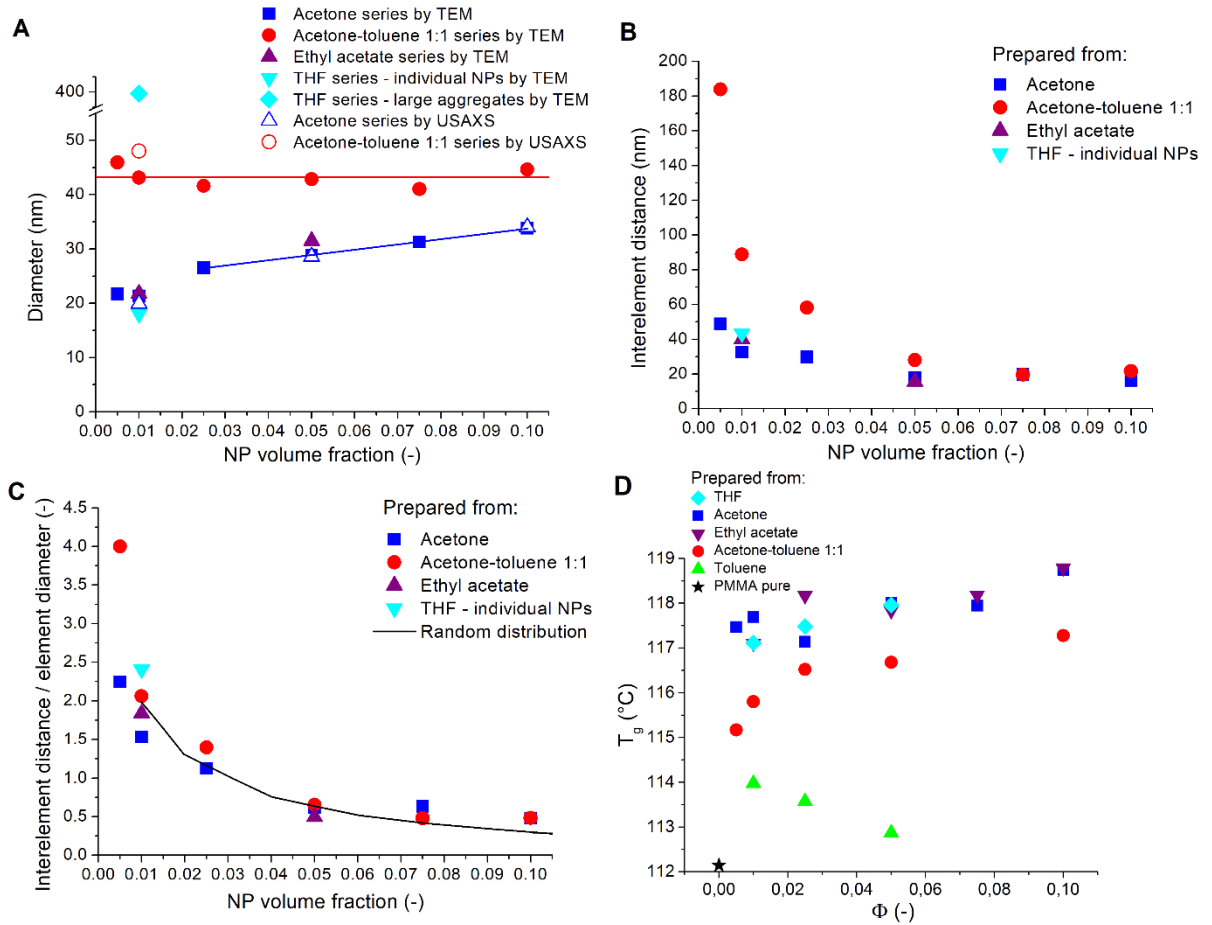


Fig. 4: Dependence of (A) element diameter according to the TEM and the USAXS, (B) interelement distance of 5 nearest neighbors determined from the automated image analysis of the TEM snapshots, and (C) interelement distance of 5 nearest neighbors divided by element diameter on NP volume fraction in solid state PNCs prepared from acetone, acetone-toluene 1:1 mixture, ethyl acetate and THF. Values for random distribution taken from the ref.¹³ (D) Glass transition temperature as a function of NP volume fraction for various NP structures.

defined as the square root of the cohesion energy density⁷³, the cohesion energy of silica could be calculated by multiplying the solubility parameter (Eq. 6) with the silica molar volume (24 cm³·mol⁻¹ for β -quartz at 848 K⁷⁶) to yield the value of 11.6 kJ·mol⁻¹. The estimate is much lower than the cohesion energy of quartz (6.52 eV \approx 629.0 kJ·mol⁻¹ for the α -modification⁷⁷) but the adsorption related processes on the nanosilica surface are not prone to change the silica molecular structure; hence, a much weaker interaction lessened by the crystallization energy is expected compared to bulk quartz. Moreover, the calculated value of the silica cohesion energy lies on the same scale as the PMMA-silica interaction strength (16.7 kJ·mol⁻¹), as shown below. This renders both the observed NP aggregation as well as the expected PMMA adsorption energetically feasible regarding the solvent choice and fortifies the correctness of the calculation. The results also support the expectation of the dominant dispersive factor with a strong polar and hydrogen bonding, which was previously observed for silica⁷⁵. However, use of some displacers led to apparently incorrect results and had to be omitted.

Table 1: The input data and the results of the silica partial solubility parameters computation, the letters (S) and (D) mark the solvent and the displacer, respectively. The solubility parameters of the solvent, the displacers and PMMA were taken from the ref.⁷³ unless otherwise stated.

	δ_D (J·cm ⁻³) ^{0.5}	δ_P (J·cm ⁻³) ^{0.5}	δ_H (J·cm ⁻³) ^{0.5}	φ_c ⁷⁵ (-)
Carbon Tetrachloride (S)	17.8	0	0.6	–
Acetone (D)	15.5	10.4	7.0	0.39
Acetonitrile (D)	15.3	18.0	6.1	0.32
Dioxane (D)	19.0	1.8	7.4	0.39
Ethyl Acetate (D)	15.8	5.3	7.2	0.85
Pyridine (D)	19.0	8.8	5.9	0.26
Tetrahydrofuran (D)	16.8	5.7	8.0	0.53
PMMA	18.6	10.5	7.5	–
PMMA ⁷⁴	18.1	10.5	5.1	–
Silica	18.8 ± 1.0	5.7 ± 0.8	6.3 ± 0.8	–

In fact, the interfacial interactions of silica NPs in PMMA solution are dominated by the acid–base interactions between acidic silanol groups on silica and basic groups of PMMA and solvents^{78–82}. The addition enthalpies were calculated according to the semi-empirical equation originally proposed by Drago, et al.⁸³ and later extended by Fowkes, et al.^{78–82} for polymers:

$$-\Delta H = E_A E_B + C_A C_B \quad (10)$$

where the parameters E and C denote the susceptibility of the acid (A) and the base (B) to undergo the electrostatic interaction and form covalent bonds, respectively. Fowkes, et al.^{78–82} found that a strong competition for the acidic moieties on the filler surface exists between a basic solvent and a basic polymer such as PMMA, while an acidic solvent would compete with acidic filler surface for basic functional groups of the polymer²⁵.

The calculated enthalpies of the donor–acceptor interactions for the model PNCs are shown in the Fig. 5A. The highest value of the negative addition enthalpy $-\Delta H_{\text{add}}$ in this study is found between THF and silanol groups on the silica surface (8.9 kcal·mol⁻¹ \approx 37.1 kJ·mol⁻¹), which is significantly stronger than the attraction between PMMA and silica (4.0 kcal·mol⁻¹ \approx 16.7 kJ·mol⁻¹). In combination with the large excess of the solvent over the polymer, it suggests that the adsorption onto silica is dominated by THF and a strong solvation shell is formed around NPs which, in turn, repels polymer chains from the vicinity of the NPs and causes NP aggregation due to the

depletion attraction. The negative addition enthalpy of silica to acetone ($6.8 \text{ kcal}\cdot\text{mol}^{-1} \approx 28.5 \text{ kJ}\cdot\text{mol}^{-1}$) and ethyl-acetate ($6.1 \text{ kcal}\cdot\text{mol}^{-1} \approx 25.6 \text{ kJ}\cdot\text{mol}^{-1}$) is smaller than to THF but still exceeds that of the silica-PMMA couple. Since solvent molecules are the enthalpically favored adsorbate, the stabilization responsible for the experimentally observed dispersion of individual NPs is likely contributed by a colloidal-like solvation effect besides the previously suggested²⁸ polymer-NP attraction induced repulsion of the adsorbed polymer shells. However, despite the NPs were preserved isolated in the ethyl acetate, slight distortion from the random distribution manifests an emerging loss of particle stability which eventually prevails at weaker NP-solvent interaction strength or at higher particle loading (see below). Unlike in the previous studies using an extremely slow solvent removal³³, the dispersion of isolated NPs obtained in the current experiments is maintained through a relatively fast solvent evaporation at $140 \text{ }^\circ\text{C}$ upon the PNC solidification. Gradually removing acetone or ethyl acetate from the liquid PNC to the point where NPs are expected to start the contact agglomeration, neighboring polymer chains enhance their chances in the competition with solvent molecules for the adsorption onto the NP surface. Viscosity of the liquid PNC progressively increases what significantly slows down the NP diffusion and, thus, reduces their ability to agglomerate. This explains the previously reported experimental results³³ stating that a fast solvent evaporation often improves NP dispersion.

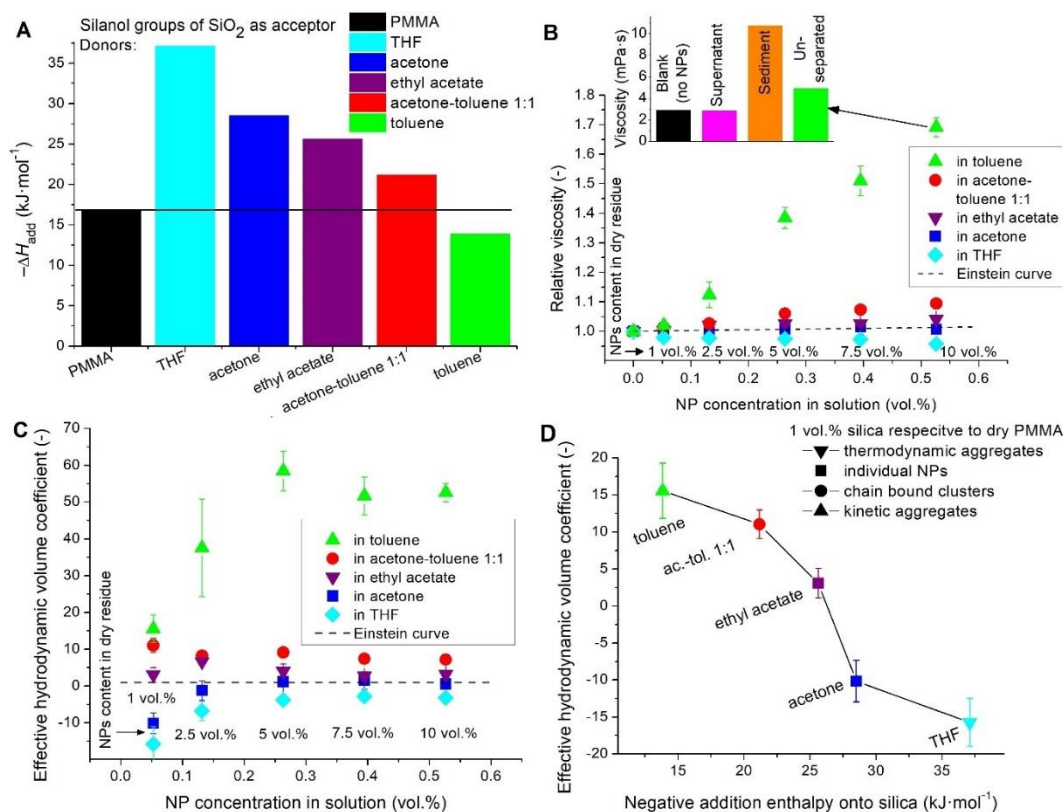


Fig. 5: (A) Bar diagram of the donor-acceptor addition enthalpies $-\Delta H_{add}$ of silanol groups of SiO_2 nanoparticles with PMMA and various solvents. The dependence of (B) the relative viscosity and (C) the effective hydrodynamic volume coefficient on the nanoparticle concentration in 5.3 vol. % solution of PMMA in various solvents with a clearly distinguishable behavior with regard to the NP spatial organization. The inset in (B) compares viscosities of the phases separated from the indicated sample by decantation. (D) Variation of the effective hydrodynamic volume with the negative addition enthalpy $-\Delta H_{add}$ of solvent onto silica for 1 vol. % silica (relative to dry PMMA) in 5.3 vol. % PMMA solution in various solvents. Symbols indicate the solid-state NP dispersion while colors match the solvents in A–C.

The strength of the interaction between the 1:1 acetone-toluene mixture and silica ($5.1 \text{ kcal}\cdot\text{mol}^{-1} \approx 21.2 \text{ kJ}\cdot\text{mol}^{-1}$) prevented the contact agglomeration; however, it was not sufficient to stabilize the dispersion of individual NPs. Since the PMMA-silica attraction is only slightly weaker than that between silica and the solvent mixture, PMMA chains may locally replace the solvent and adsorb onto the NP surface. This balanced competition between the polymer and solvent adsorption is proposed as the mechanism by which the chain bound NP clusters are formed (Fig. 3D). The low negative enthalpy of addition between toluene and silica ($3.3 \text{ kcal}\cdot\text{mol}^{-1} \approx 13.8 \text{ kJ}\cdot\text{mol}^{-1}$) is reflected by the inability of the solvent to stabilize the dispersed NPs by solvation what leads to the contact agglomeration. The strength of the attraction between PMMA and silica is greater than that for the toluene-silica interaction ($3.3 \text{ kcal}\cdot\text{mol}^{-1} \approx 13.8 \text{ kJ}\cdot\text{mol}^{-1}$) which suggests that the polymer adsorption onto the NP surface takes place as a competitive process to the contact aggregation since the weak toluene-silica interaction is incapable to stabilize the predispersed NPs. The competition is manifested by the presence of two populations of ensembles in the TEM images (Fig. 3E).

While not capable to directly determine the final structure, rheological data (Fig. 5B) provides valuable supplementary information that sheds new light to the structuring phenomena. In the simplest form, the relative viscosity η_r of a dilute suspension of monodisperse spheres is predicted by the Einstein's formula and is only relevant to the particle hydrodynamic volume, i.e., the effective volume of hydrodynamic constraints experienced by the flow due to the presence of the particles. The hydrodynamic volume typically accounts for the combined volume of bare particles ϕ and various solvation effects. If those two contributions are separated, the latter is usually merged with the Einstein's constant and referred to as the intrinsic viscosity or it could be described as the effective hydrodynamic volume coefficient k (Fig. 5C), defined as the ratio of the intrinsic viscosity and the Einstein's value of 2.5 (Eq. 1). The effective volume could be comprehended as the volume required to address the actual viscosity regarding the volume fraction of bare particles in the constraints of the Einstein's equation where the value of 1 relates to systems obeying the Einstein's formula whereas smaller and larger values pertain to the sub- and super-Einstein behavior, respectively. All three cases are eligible and strongly correlated to the structure of polymer nanocomposite fluid³⁶.

A systematic S-shaped decrease of the effective hydrodynamic volume coefficient with the increasing $-\Delta H_{\text{add}}$ of the solvent adsorption onto the silica was observed (Fig. 5D). The data reflects a shift from the favorable polymer adsorption at large positive k in weakly interacting solvents such as toluene or acetone-toluene 1:1 mixture to the prevalent depletion attraction at large negative k in high-affine acetone and THF. Notably, no systematic trend between the value of k or the final NP dispersion and the dielectric properties nor zeta potentials was observed. Clearly, the agglomeration in THF and toluene are two unlike processes of dissimilar origin since the interaction strengths of both solvents with silica stand on the opposite sides of the range investigated in this work. The kinetics of both processes was recorded by adding predispersed NPs directly into the rheometer geometry (Fig. 6B). In THF, the initial drop in the relative viscosity partially smeared out over the time what reflects the declining depletion attraction as the effective surface area of the NPs decreased with the proceeding aggregation. Simultaneously, the aggregation also prolonged the mean separation distance that further promoted the stability of the remaining NPs. The combined presence of aggregates and individual NPs suggests a nucleation mechanism of the aggregate growth in THF where the process is kinetically limited by the number of the available nuclei which attract single NPs from their vicinity until a certain critical size is reached or, speculatively, the aggregation tendency is exhausted. The slight increase of the relative viscosity is highly unlikely attributed to the solvent evaporation since it was not present in blank samples, i.e., polymer solution without NPs. In toluene, the agglomeration took place rapidly, practically instantly. The observed change was completed in about the same time ($\sim 2 \text{ s}$) as was required for mixing the predispersed NPs into the

polymer solution with a pipette which means that the process is presumably kinetically controlled by the rate of NP addition. The following decay of the viscosity was caused by a sedimentation of large agglomerates which rendered them unavailing to the concentric cylinder geometry. A fully sedimented sample was decanted and the phases were tested separately but no presence of NPs was found in the supernatant by thermogravimetric analysis while its viscosity was slightly reduced compared to the pure polymer solution (Fig. 5B inset), suggesting that the NPs separated into a viscous particle-rich phase thick with polymer. The high recorded viscosity of unseparated samples is in fact an intermediate value of these two phases and as such was inadequate to be addressed by the simple approach based on the Einstein's formula. The phase separation correlates well with the deteriorated homogeneity of the NP distribution observed in the TEM images.

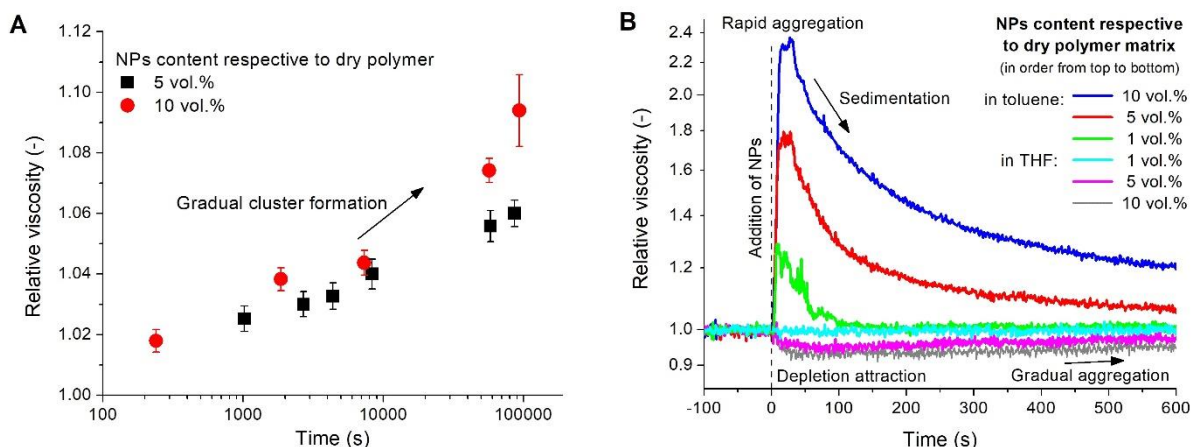


Fig. 6: (A) A slow formation kinetics of chain-bound NP clusters in 5.3 vol. % PMMA solution in acetone-toluene 1:1 mixture. Each point represents an independent sample. (B) A more rapid formation of kinetical and thermodynamic aggregates in 5.3 vol. % PMMA solution in toluene and THF, respectively. The former is accompanied by a rapid gain in the relative viscosity due to the evolved structures whereas the latter is manifested by a less pronounced decrease of the viscosity due to the depletion attraction which partially diminishes as the aggregation proceeds. Each line represents an average of two independent measurements in which predispersed NPs were added directly into the rheometer geometry. The logarithmic scale is employed to better visualize the comparison of both processes.

Acetone-toluene 1:1 mixture has the second weakest interaction with silica out of the investigated solvents but unlike the rapid contact agglomeration in toluene, the relative viscosity of the cluster forming nanocomposite solutions gradually rose with time (Fig. 6A). The relative increment exceeded the prediction of the Einstein's equation nearly ten times after one day (Fig. 5B–C). Considering an even spacing of the additional hydrodynamic volume around each particle, the NPs in clusters would have to be enlarged by about 19–22 nm in the diameter to ascribe the excess viscosity. Despite this approach being over simplistic, it draws a conclusion that the average thickness of the adsorbed layer is approximately $1 R_G$ which correlates reasonably well with the literature reports^{43,47,84}.

Rheological measurements also indicated that the solvation stabilization in acetone where a weak depletion attraction was detected smoothly shifts into the adsorption of polymer layers in ethyl acetate and acetone-toluene 1:1. An interpolation between the former two solvents reveals that the ideal Einstein's behavior would be reached at $-\Delta H_{\text{add}}$ around $-6.2 \text{ kcal}\cdot\text{mol}^{-1} \approx -25.9 \text{ kJ}\cdot\text{mol}^{-1}$, $2.2 \text{ kcal}\cdot\text{mol}^{-1} \approx 9.2 \text{ kJ}\cdot\text{mol}^{-1}$ below the addition enthalpy of PMMA-silica ($-4.0 \text{ kcal}\cdot\text{mol}^{-1} \approx -16.7 \text{ kJ}\cdot\text{mol}^{-1}$). For comparison, the difference of the silica cohesion energy ($-11.6 \text{ kJ}\cdot\text{mol}^{-1}$, see above) and the PMMA-silica addition enthalpy takes the value of $5.1 \text{ kJ}\cdot\text{mol}^{-1}$. Given the fact that the entropic penalty upon adsorption on a nanoparticle diminishes with increasing chain length of the adsorbate^{71,85}, it is reasonable to expect that the full desorption of a polymer by a much smaller

solvent molecule requires the latter to show an enthalpic gain superior to that of the polymer to outweigh the higher entropic penalty. Following this idea, one could attribute the value of $9.2 \text{ kJ}\cdot\text{mol}^{-1}$ to the entropic gain as solvent is swapped with PMMA as the adsorbate on nanosilica. Despite the polymer chain itself experience an unfavorable adsorption entropy^{7,71,86}, the overall entropic situation is beneficial to the polymer adsorption from solution. This conclusion correlates with the experimental findings of Hamieh⁸⁷ who reported the specific entropy of adsorption of PMMA-SiO₂ from various solvents to lie in the range $0-62 \text{ J}\cdot\text{K}^{-1}\cdot\text{mol}^{-1} \approx 0-18.5 \text{ kJ}\cdot\text{mol}^{-1}$ @ $25 \text{ }^\circ\text{C}$, among which toluene and THF take the value of 4 and $60 \text{ J}\cdot\text{K}^{-1}\cdot\text{mol}^{-1}$, respectively. Remarkably, the currently estimated value of $9.2 \text{ kJ}\cdot\text{mol}^{-1}$ is found near the middle of the range. However, the strong dependence of the adsorption entropy on solvent⁸⁷ prevents any further generalization of the results.

In an attempt to compare the current experimental data with the PRISM theory by Schweizer⁷, the addition enthalpy $-H_{\text{add}}$ (Fig. 5D) was converted into interaction strength (Fig. 8E). An adsorption of a dissolved polymer onto a NP requires that the active sites of both the polymer and the NP surface are freed of the solvent molecules that previously occupied them. Hence, the combined NP-solvent and solvent-polymer interaction opposes the polymer adsorption onto the NP surface while the freed solvent molecules reestablish a mutual interaction. Therefore, the interaction strength was calculated by subtracting the polymer-solvent enthalpy of mixing obtained from the Hansen's solubility parameters:

$$\Delta H_{\text{mix}} = RT\chi = \frac{V_m}{4} (\text{Ra})^2 \quad (11)$$

where χ , V_m and Ra denote the Flory-Huggins interaction parameter, molar volume and Hansen's distance parameter (eq. 5), respectively; and the solvent-silica addition enthalpy from the sum of the PMMA-silica addition enthalpy and solvent cohesion (evaporation) enthalpy $\Delta H_{\text{evap.}}$. Unlike the PRISM theory deducted for polymer melts, the current experimental system is fairly diluted what mitigates the internal interactions³⁴ and reduces the number of entanglement per chain⁸⁸; hence, the calculated value was multiplied by the polymer volume ratio ($\varphi_p = 0.053$) to incorporate the dilution effect and receive the overall interaction strength:

$$\varepsilon = -\Delta H \cdot \varphi_p = -\varphi_p (\Delta H_{\text{add., p-NP}} + \Delta H_{\text{evap., s}} - \Delta H_{\text{add., s-NP}} - \Delta H_{\text{mix, p-s}}) \quad (12)$$

where the subscripts 'p' and 's' mark polymer and solvent, respectively. Remarkably, this rather complex computation combined with the experimental data for the non-aggregated samples collapses into a perfect line with the coefficient of determination $R^2 = 0.9999$ (Fig. 8E). An interpolation of the acetone and ethyl acetate data showed that the ideal Einstein's behavior would be reached at $-27.0 \text{ kJ}\cdot\text{mol}^{-1}$.

The results, presented in the Table 4 along with the input parameters, were transformed into a phase diagram (Fig. 8F) predicted by the PRISM theory⁷ for polymer chains of $N = 100$ mers, decay length of the interaction $\alpha = 0.5$ and variable NP-mer size ratio D/d . The number average molecular weight of the PMMA used in the experiments was $50 \text{ kg}\cdot\text{mol}^{-1}$ which means that an average chain contains ~ 500 methyl methacrylate units. Provided the length of a C-C bond being 0.154 nm , the D/d would take the value of ~ 65 . If, however, a Kuhn's segment would be considered as the basic chain unit, an average chain would contain ~ 100 units (Kuhn's length of PMMA equals $l_K = 1.53 \text{ nm}$ ⁸⁹) and the D/d ratio would drop to ~ 13 , both being values in the range investigated by the reported simulation. Keeping in mind the unclarity how well the simulation parameters match the current experimental system, a very good correlation was found between the model and the experimental structures at weak interaction strengths (depletion-driven phase separation). The chain-bound clusters lie deep in the miscible window though, but that could further shrink with an increasing D/d ratio or a decreasing decay length α ⁷. Speculatively, the entropically driven depletion

aggregation treats the Kuhn’s segment as the primary chain unit as it is a better representative of the chain dynamics while the enthalpically driven formation of polymer-bound clusters seems to conform better to monomer being the elementary chain unit, possibly due to the adsorption taking place on the scale of individual atoms and functional groups. However, one cannot omit the fact that the presence of solvent transforms the entropic contribution from unfavorable to favorable, as discussed above, which was not considered in the original PRISM theory.

Table 2: Overview of addition enthalpy onto silica ΔH_{add} , cohesion (evaporation) enthalpy $\Delta H_{evap.}$, mixing enthalpy obtained from the HSP solubility parameters ΔH_{mix} , undiluted interaction enthalpy of PMMA-silica ΔH , and diluted interaction strength $\varepsilon = -\Delta H \cdot \phi_P$ for PMMA and various solvents.

	ΔH_{add} (kJ·mol ⁻¹)	$\Delta H_{evap.}$ (kJ·mol ⁻¹)	ΔH_{mix} (kJ·mol ⁻¹)	ΔH (kJ·mol ⁻¹)	$\varepsilon = -\Delta H \cdot \phi_P$ (kJ·mol ⁻¹)	$\varepsilon = -\Delta H \cdot \phi_P$ (k _B ·T)
THF	-37.1	-32.0	0.78	-12.38	0.65	0.26
acetone	-28.5	-33.7	0.56	-22.61	1.19	0.48
ethyl acetate	-25.6	-35.9	1.29	-28.42	1.49	0.60
acetone-toluene 1:1	-21.2	-35.6	0.67	-32.02	1.68	0.68
toluene	-13.8	-38.0	2.46	-43.67	2.30	0.93
PMMA	-16.7	-	-	-	-	-

Finally, the glass transition temperature (T_g) was chosen as an exemplary bulk property of PNC to demonstrate the importance of NP spatial organization (Fig. 5D). Addition of NPs led to elevated T_g compared to pure PMMA in all cases regardless the NP structure. According to the expectations, the highest increase of T_g (~6 °C) was recorded for individually dispersed NPs (prepared from acetone or ethyl-acetate) which provided largest NP surface area available for polymer adsorption. The increase of T_g scaled only very weakly with NP volume fraction in these samples which means that the majority of polymer chains were already affected by addition of small portion of dispersed NPs. If the mean separation length of NP elements drops below approximately 4 times the polymer coil diameter, i.e., about 40 nm in this case, each chain is statistically either adjacent to a NP or neighboring with a such chain. Adsorption on NP surface alters the chain dynamics which in turn influences the dynamics of an intertangled neighbor. This possibly explains the nearly identical values of T_g for samples with individually dispersed NPs with the samples prepared from THF – though large aggregates were present; the remaining NPs were evenly dispersed through the matrix at mean interparticle distance comparable to the samples of acetone and ethyl acetate series (Fig. 4B) and probably contributed to most of the observed increase in T_g . Contrary, clusters of acetone-toluene 1:1 series showed systematically rising T_g with increasing NP volume fraction which manifested the constrained NP surface area available for polymer adsorption and extended mean separation length between clusters. The heterogeneous character of samples prepared from toluene, uneven distribution of NPs throughout the matrix due to phase separation and effective NP surface area lessened by aggregation reduced the impact of NPs on the polymer matrix and caused the samples of toluene series to exhibit the lowest T_g out of all the investigated PNCs. (prepared from acetone or ethyl-acetate) which provided largest NP surface area available for polymer adsorption. The increase of T_g scaled only very weakly with NP volume fraction in these samples which means that the majority of polymer chains were already affected by addition of small portion of dispersed NPs. If the mean separation length of NP elements drops below approximately 4 times the polymer coil diameter, i.e., about 40 nm in this case, each chain is statistically either adjacent to a NP or

neighboring with a such chain. Adsorption on NP surface alters the chain dynamics which in turn influences the dynamics of an intertangled neighbor. This possibly explains the nearly identical values of T_g for samples with individually dispersed NPs with the samples prepared from THF – though large aggregates were present; the remaining NPs were evenly dispersed through the matrix at mean interparticle distance comparable to the samples of acetone and ethyl acetate series (Fig. 4B) and probably contributed to most of the observed increase in T_g . Contrary, clusters of acetone-toluene 1:1 series showed systematically rising T_g with increasing NP volume fraction which manifested the constrained NP surface area available for polymer adsorption and extended mean separation length between clusters. The heterogeneous character of samples prepared from toluene, uneven distribution of NPs throughout the matrix due to phase separation and effective NP surface area lessened by aggregation reduced the impact of NPs on the polymer matrix and caused the samples of toluene series to exhibit the lowest T_g out of all the investigated PNCs.

6.2. Silica in polystyrene

A set of PS/silica samples was prepared (Fig. 7) to elaborate on the general applicability of the results obtained with PMMA/silica nanocomposites. The silica NPs predispersed in ethyl methyl ketone remained individually dispersed when added to THF, *N,N*-dimethylacetamide (DMAc) and cyclohexanone. 1 vol.% of silica NPs maintained a clustered spatial organization in DMAc ($d_{\text{mean}} = 33.8$ nm) and cyclohexanone ($d_{\text{mean}} = 36.5$ nm) while depletion aggregation occurred in THF ($d_{\text{mean}} = 1804.6$ nm), but, unlike in PMMA nanocomposites, no evidence of individual NPs alongside the large aggregates was found in the samples prepared from THF (Fig. 7 III). A rather vague correlation of the interelement distance of the 5 nearest neighbors to the element diameter ratio was found between the experimental structures and a random dispersion (Fig. 8A); however, the steep slope at the low NP loading limit renders the function very sensitive to the precise particle content and, thus, prone to be dominated by the local NP concentration fluctuation.

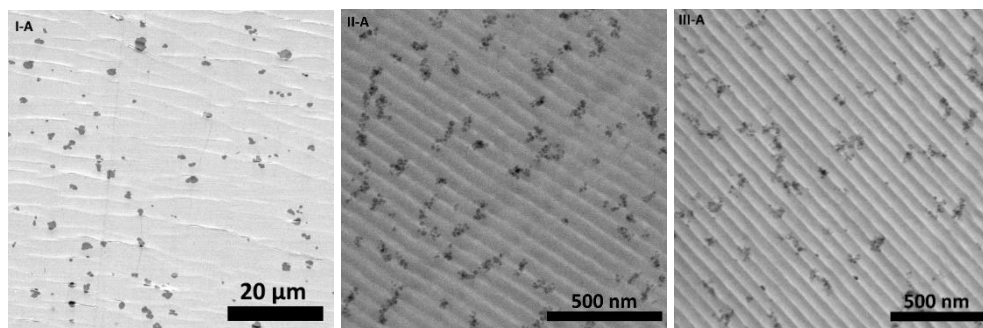


Fig. 7: STEM images of silica in PS 192k, **(I)** THF/1 vol. % silica, **(II)** DMAc/1 vol. % silica, **(III)** cyclohexanone/1 vol. % silica.

The addition enthalpies onto silica were calculated according to the Drago's concept from the eq. 10 (Fig. 8B, Table 5). The missing values for cyclohexanone were substituted by acetone as the chemically closest substance with available data and the value for PS was approximated from styrene (substituted by toluene) multiplied by the polymer/monomer ratio for PMMA/MMA (substituted by methyl acetate) considering that the effectivity of the polymer interactions relative to its monomer is similar for PS and PMMA and stems from the steric inaccessibility of the functional groups attached to the polymer backbone. The depletion aggregation and clustering caused analogical discrepancy between the recorded viscosity (Fig. 8C) and the theoretical prediction of the Einstein's model (Fig. 8D) as their PMMA counterparts. At the first glance, the dissimilarity of the

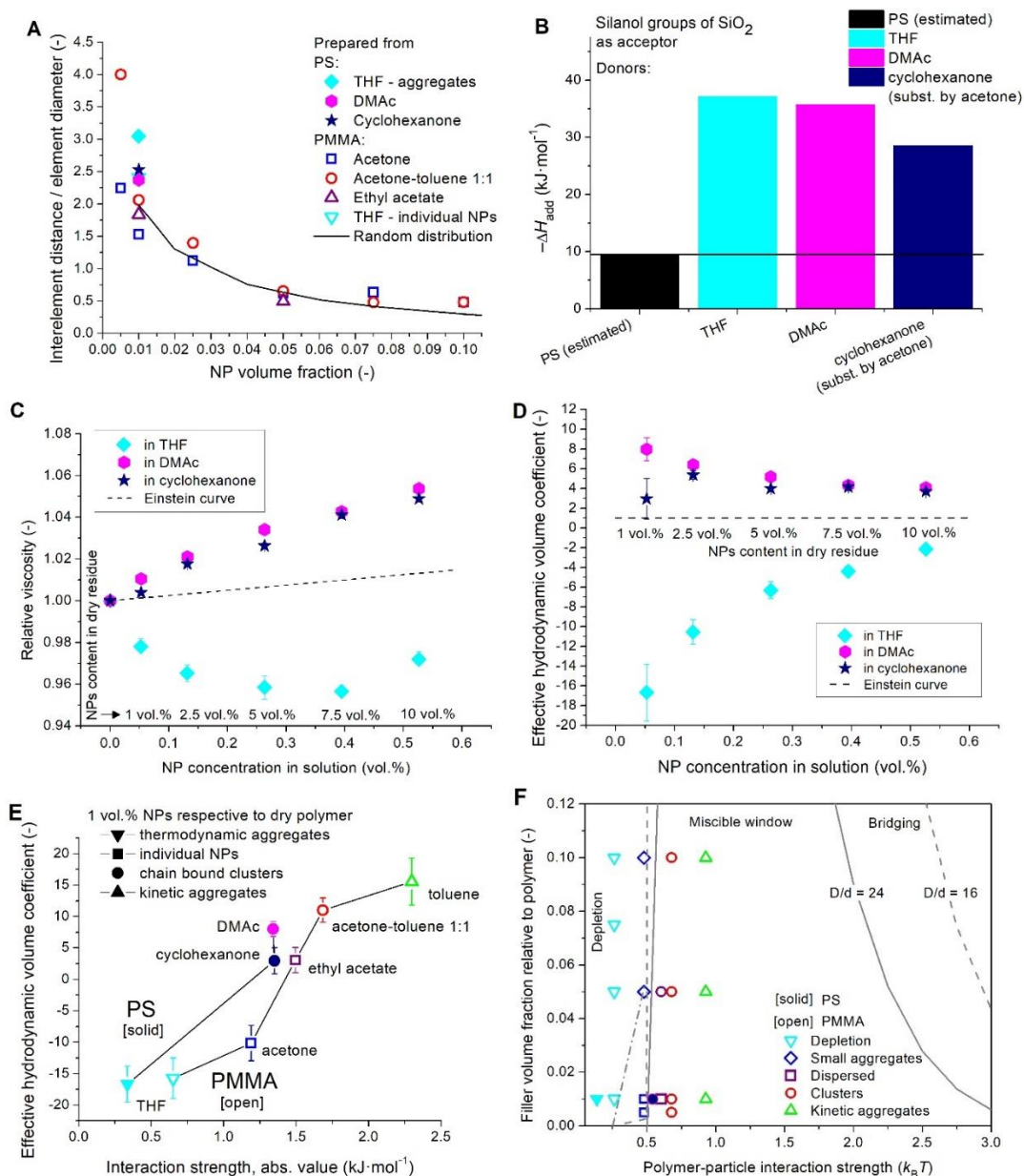


Fig. 8: (A) Dependence of interelement distance of 5 nearest neighbors divided by element diameter on NP volume fraction in solid state PS-based PNCs prepared from THF, DMAc, and cyclohexanone compared to PMMA PNCs. (B) Bar diagram of the donor-acceptor addition enthalpies $-\Delta H_{add}$ of silanol groups of SiO₂ nanoparticles with PS and various solvents. The dependence of (C) the relative viscosity and (D) the effective hydrodynamic volume coefficient on the nanoparticle concentration in 5.3 vol. % solution of PS in various solvents with a clearly distinguishable behavior regarding the NP spatial organization. (E) Comparison of the effective hydrodynamic volume variation with the interaction strength ϵ (Eq. 12) between solvent and silica at 1 vol. % NP content (relative to dry polymer) for PMMA and PS 5.3 vol. % solution in various solvents. Symbols indicate the solid-state NP dispersion while colors match the solvents in A–D. (F) Phase diagram of PMMA-silica (open symbols) and PS-silica (solid symbols) nanocomposites. Current experiments (points) are compared with the prediction of the PRISM theory (lines) presented in the ref. ⁷. Symbols indicate the solid-state NP dispersion while colors mark matching solvents in A–E.

experimental structures, clearly proved by both the electron microscopy (Fig. 7) and the rheological data (Fig. 8C–D), might look confusing given the close values of the addition enthalpies on silica for THF ($-8.9 \text{ kcal}\cdot\text{mol}^{-1} \approx -37.1 \text{ kJ}\cdot\text{mol}^{-1}$) and DMAc ($-8.5 \text{ kcal}\cdot\text{mol}^{-1} \approx -35.7 \text{ kJ}\cdot\text{mol}^{-1}$);

however, the interaction strength calculated according to the eq. 12 revealed the unlike character of the PS-silica interaction in these two solvents (Table 3) and both the depletion aggregation and clustering occurred in similar range as in the PMMA samples (Fig. 8E). It is worth noting that the PMMA/silica in ethyl acetate, system with the closest interaction strength to the clustered PS/silica in DMAc and cyclohexanone, showed a dispersion of individual NPs at 1 vol. % with a distorted distribution, possibly due to attractive interparticle interaction, and a possible clustering at 5 vol. %. The phase diagram in the Fig. 8F suggests that the PS further narrows the miscible window, which would be expected for a longer polymer chain with a shorter Kuhn's length (1.0 nm for PS⁹⁰ compared to 1.53 nm for PMMA) defined by $N \approx 280$, and $D/d \approx 20$.

Table 3: Overview of addition enthalpy onto silica ΔH_{add} , cohesion (evaporation) enthalpy $\Delta H_{evap.}$, mixing enthalpy obtained from the HSP solubility parameters ΔH_{mix} , undiluted interaction enthalpy of PS-silica ΔH , and diluted interaction strength $\varepsilon = -\Delta H \cdot \phi_P$ for PS and various solvents.

	ΔH_{add} (kJ·mol ⁻¹)	$\Delta H_{evap.}$ (kJ·mol ⁻¹)	ΔH_{mix} (kJ·mol ⁻¹)	ΔH (kJ·mol ⁻¹)	$\varepsilon = -\Delta H \cdot \phi_P$ (kJ·mol ⁻¹)	ε (k _B ·T)
THF	-37.1	-32.0	1.94	-6.36	0.33	0.14
DMAc	-35.7	-48.2	3.45	-25.50	1.34	0.54
cyclohexanone	-28.4	-43.1	1.47	-25.66	1.35	0.54
PS	-9.5	-	-	-	-	-

7. Conclusions

NP structuring phenomena in polymer matrix was studied on silica/PMMA model system and the general applicability of the conclusions was tested on silica/PS samples. The adopted solution blending method was recognized as a suitable technique of polymer nanocomposite (PNC) preparation capable of simple nanoparticle (NP) dispersion tuning by the selection of solvent. A promising potential for further applications was promoted by preserving the NP spatial organization through the excessive thermal processing. Qualitative differences between various NP spatial organizations (individually dispersed NPs, polymer bound clusters and aggregates) were investigated with emphasis on the impact of NP dispersion on PNC properties which were demonstrated by direct comparison of glass transition temperatures for various NP arrangements. Deeper investigation into the structural impact on relaxation and mechanical properties may represent a goal for the further research. Combined results of TEM image analysis, USAXS and rheology provided a complex image of physico-chemical principles controlling the structuring phenomena of nanoparticles in polymer solutions and brought a comprehensive understanding of the composition-preparation protocol-solid state structure relationship.

Experimental evidence suggesting that the NP dispersion state is inherited from the solution-blending step of the PNC preparation and stems from the complex interplay of solvent-solvent, solvent-polymer, solvent-particle, polymer-particle, and particle-particle attractions was provided. The processing solvent was quantitatively linked to the amount of polymer adsorption and depletion attraction through a systematic increase of the effective hydrodynamic volume coefficient k with the increasing polymer-silica interaction strength which in turn depended strongly on the solvent's physico-chemical properties. A major contribution was attributed to the basic properties of the solvent molecule competing with the basic functional groups of polymer segments for the acidic active sites on the silica surface. The data reflects a shift from a favorable polymer adsorption at large positive k in weakly interacting solvents such as toluene or acetone-toluene 1:1 for PMMA and DMAc or cyclohexanone for PS mixture to a prevalent depletion attraction at large negative k in

high-affine acetone or THF. An ideal Einstein behavior of the silica/PMMA nanocomposite solution was predicted by interpolation between acetone and ethyl acetate to occur in a solvent in which the PMMA would experience an interaction strength to silica of $-27.0 \text{ kJ}\cdot\text{mol}^{-1}$. The experimental results correlated rather well with the prediction of the PRISM theory when dilution of the interaction strength was considered, since the theory was originally developed for adsorbing nanocomposite melts. A very narrow miscibility window was observed though, and it even closed at higher particle concentration. These results could potentially serve as the basis for prediction of the outcoming NP dispersion in adsorbing solution blended PNCs which could find an application in the design of advanced polymer nanocomposites with enhanced functional properties.

8. References

- 1 L. J. Gibson, *J. R. Soc. Interface*, 2012, **9**, 2749–2766.
- 2 F. Barthelat and M. Engineering, *Philos. Trans. R. Soc. London A Math. Phys. Eng. Sci.*, 2007, **365**, 2907–2919.
- 3 U. G. K. Wegst, H. Bai, E. Saiz, A. P. Tomsia and R. O. Ritchie, *Nat. Mater.*, 2014, **14**, 23–36.
- 4 H. D. Espinosa, J. E. Rim, F. Barthelat and M. J. Buehler, *Prog. Mater. Sci.*, 2009, **54**, 1059–1100.
- 5 J.-Y. Rho, L. Kuhn-Spearing and P. Zioupos, *Med. Eng. {&} Phys.*, 1998, **20**, 92–102.
- 6 J. Wang, Q. Cheng and Z. Tang, *Chem. Soc. Rev.*, 2012, **41**, 1111–1129.
- 7 J. B. Hooper and K. S. Schweizer, *Macromolecules*, 2006, **39**, 5133–5142.
- 8 G. Nichols, S. Byard, M. J. Bloxham, J. Botterill, N. J. Dawson, A. Dennis, V. Diart, N. C. North and J. D. Sherwood, *J. Pharm. Sci.*, 2002, **91**, 2103–2109.
- 9 L. M. Sherman, *Plast. Technol.*, 2004, **50**, 56–61.
- 10 F. W. Starr, J. F. Douglas and S. C. Glotzer, *J. Chem. Phys.*, 2003, **119**, 1777.
- 11 P. C. Hiemenz and R. Rajagopalan, *Principles of Colloid and Surface Chemistry, Third Edition, Revised and Expanded*, CRC Press, 1997.
- 12 S. H. Donaldson, A. Røyne, K. Kristiansen, M. V Rapp, S. Das, M. A. Gebbie, D. W. Lee, P. Stock, M. Valtiner and J. Israelachvili, *Langmuir*, 2015, **31**, 2051–2064.
- 13 J. Zidek, J. Kucera and J. Jancar, *C. Mater. Contin.*, 2011, **24**, 183–208.
- 14 S. Torquato and Y. Jiao, *Phys. Rev. E. Stat. Nonlin. Soft Matter Phys.*, 2012, **86**, 11102.
- 15 J. Jancar, J. F. Douglas, F. W. Starr, S. K. Kumar, P. Cassagnau, A. J. Lesser, S. S. Sternstein and M. J. Buehler, *Polymer (Guildf.)*, 2010, **51**, 3321–3343.
- 16 A. Hashemi, N. Jouault, G. A. Williams, D. Zhao, K. J. Cheng, J. W. Kysar, Z. Guan and S. K. Kumar, *Nano Lett.*, 2015, **15**, 5465–5471.
- 17 D. Maillard, S. K. Kumar, B. Fragneaud, J. W. Kysar, A. Rungta, B. C. Benicewicz, H. Deng, L. C. Brinson and J. F. Douglas, *Nano Lett.*, 2012, **12**, 3909–3914.
- 18 J. Jordan, K. I. Jacob, R. Tannenbaum, M. A. Sharaf and I. Jasiuk, *Mater. Sci. Eng. A*, 2005, **393**, 1–11.
- 19 D. Zhao, D. Schneider, G. Fytas and S. K. Kumar, *ACS Nano*, 2014, **8**, 8163–8173.
- 20 S. E. Harton, S. K. Kumar, H. Yang, T. Koga, K. Hicks, H. Lee, J. Mijovic, M. Liu, R. S. Vallery and D. W. Gidley, *Macromolecules*, 2010, **43**, 3415–3421.
- 21 L. S. Schadler, S. K. Kumar, B. C. Benicewicz, S. L. Lewis and S. E. Harton, *MRS Bull.*, 2007, **32**, 335–340.
- 22 S. Y. Kim, K. S. Schweizer and C. F. Zukoski, *Phys. Rev. Lett.*, 2011, **107**, 225504.
- 23 J. S. Meth, S. G. Zane, C. Chi, J. D. Londono, B. A. Wood, P. Cotts, M. Keating, W. Guise and S. Weigand, *Macromolecules*, 2011, **44**, 8301–8313.
- 24 D. W. Janes, J. F. Moll, S. E. Harton and C. J. Durning, *Macromolecules*, 2011, **44**, 4920–

- 4927.
- 25 A. Bansal, H. Yang, C. Li, K. Cho, B. C. Benicewicz, S. K. Kumar and L. S. Schadler, *Nat. Mater.*, 2005, **4**, 693–698.
 - 26 D. B. Stojanović, L. Brajović, A. Orlović, D. Dramlić, V. Radmilović, P. S. Uskoković and R. Aleksić, *Prog. Org. Coatings*, 2013, **76**, 626–631.
 - 27 C. Triebel and H. Münstedt, *Polymer (Guildf.)*, 2011, **52**, 1596–1602.
 - 28 M. E. Mackay, A. Tuteja, P. M. Duxbury, C. J. Hawker, B. Van Horn, Z. Guan, G. Chen and R. S. Krishnan, *Science (80-.)*, 2006, **311**, 1740–1743.
 - 29 D. Cangialosi, V. M. Boucher, A. Alegría and J. Colmenero, *Polymer (Guildf.)*, 2012, **53**, 1362–1372.
 - 30 N. Jouault, P. Vallat, F. Dalmas, S. Said, J. Jestin and F. Boué, *Macromolecules*, 2009, **42**, 2031–2040.
 - 31 N. Jouault, F. Dalmas, F. Boué and J. Jestin, *Polymer (Guildf.)*, 2012, **53**, 761–775.
 - 32 C. Chevigny, N. Jouault, F. Dalmas, F. Boué and J. Jestin, *J. Polym. Sci. Part B Polym. Phys.*, 2011, **49**, 781–791.
 - 33 N. Jouault, D. Zhao and S. K. Kumar, *Macromolecules*, 2014, **47**, 5246–5255.
 - 34 S. Y. Kim and C. F. Zukoski, *Langmuir*, 2011, **27**, 10455–10463.
 - 35 S. Y. Kim and C. F. Zukoski, *Langmuir*, 2011, **27**, 5211–5221.
 - 36 S. Y. Kim and C. F. Zukoski, *Soft Matter*, 2012, **8**, 1801–1810.
 - 37 A. . Nakatani, W. Chen, R. . Schmidt, G. . Gordon and C. . Han, *Polymer (Guildf.)*, 2001, **42**, 3713–3722.
 - 38 A. Tuteja, P. M. Duxbury and M. E. Mackay, *Phys. Rev. Lett.*, 2008, **100**, 077801.
 - 39 S. Y. Kim, H. W. Meyer, K. Saalwächter and C. F. Zukoski, *Macromolecules*, 2012, **45**, 4225–4237.
 - 40 J. B. Hooper, K. S. Schweizer, T. G. Desai, R. Koshy and P. Keblinski, *J. Chem. Phys.*, 2004, **121**, 6986.
 - 41 J. B. Hooper and K. S. Schweizer, *Macromolecules*, 2005, **38**, 8858–8869.
 - 42 J. B. Hooper and K. S. Schweizer, *Macromolecules*, 2007, **40**, 6998–7008.
 - 43 B. J. Anderson and C. F. Zukoski, *Macromolecules*, 2009, **42**, 8370–8384.
 - 44 T. Jiang and C. F. Zukoski, *Macromolecules*, 2012, **45**, 9791–9803.
 - 45 S. Y. Kim and C. F. Zukoski, *Macromolecules*, 2013, **46**, 6634–6643.
 - 46 M. Ranka, N. Varkey, S. Ramakrishnan and C. F. Zukoski, *Soft Matter*, 2015, **11**, 1634–1645.
 - 47 B. J. Anderson and C. F. Zukoski, *Macromolecules*, 2008, **41**, 9326–9334.
 - 48 B. J. Anderson and C. F. Zukoski, *Langmuir*, 2010, **26**, 8709–8720.
 - 49 S. Wu, R. B. Ladani, J. Zhang, E. Bafekrpour, K. Ghorbani, A. P. Mouritz, A. J. Kinloch and C. H. Wang, *Carbon N. Y.*, 2015, **94**, 607–618.
 - 50 Q. Zhang, M. Janner, L. He, M. Wang, Y. Hu, Y. Lu and Y. Yin, *Nano Lett.*, 2013, **13**, 1770–1775.
 - 51 R. B. Ladani, S. Wu, A. J. Kinloch, K. Ghorbani, J. Zhang, A. P. Mouritz and C. H. Wang, *Mater. Des.*, 2016, **94**, 554–564.
 - 52 P. K. Khanna, N. Singh, S. Charan, V. V. V. S. Subbarao, R. Gokhale and U. P. Mulik, *Mater. Chem. Phys.*, 2005, **93**, 117–121.
 - 53 J. Ž. Kuljanin-Jakovljević, A. N. Radosavljević, J. P. Spasojević, M. V. Carević, M. N. Mitrić and Z. M. Kačarević-Popović, *Radiat. Phys. Chem.*, 2017, **130**, 282–290.
 - 54 Y. Lu, Y. Mei, M. Schrunner, M. Ballauff, M. W. Möller and J. Brey, *J. Phys. Chem. C*, 2007, **111**, 7676–7681.
 - 55 A. Fina, D. Tabuani and G. Camino, *Eur. Polym. J.*, 2010, **46**, 14–23.
 - 56 M. Sánchez-Soto, D. A. Schiraldi and S. Illescas, *Eur. Polym. J.*, 2009, **45**, 341–352.
 - 57 S. Iyer and D. A. Schiraldi, *Macromolecules*, 2007, **40**, 4942–4952.

- 58 M. Joshi, B. S. Butola, G. Simon and N. Kukaleva, *Macromolecules*, 2006, **39**, 1839–1849.
- 59 P. Cassagnau, *Polymer (Guildf.)*, 2003, **44**, 2455–2462.
- 60 Y. Zheng, K. Yan, Y. Zhao, X. Zhu, M. Möller and C. Hu, *Fibers Polym.*, 2016, **17**, 2020–2026.
- 61 J. Alvarado, G. Acosta and F. Perez, *Polym. Degrad. Stab.*, 2016, **134**, 376–382.
- 62 R. Shenhar, T. B. Norsten and V. M. Rotello, *Adv. Mater.*, 2005, **17**, 657–669.
- 63 N. Jouault, M. K. Crawford, C. Chi, R. J. Smalley, B. Wood, J. Jestin, Y. B. Melnichenko, L. He, W. E. Guise and S. K. Kumar, *ACS Macro Lett*, 2016, **5**, 523–527.
- 64 S. Mueller, E. W. Llewellyn and H. M. Mader, *Proc. R. Soc. A Math. Phys. Eng. Sci.*, 2009, **466**, 1201–1228.
- 65 L. M. Hall, A. Jayaraman and K. S. Schweizer, *Curr. Opin. Solid State Mater. Sci.*, 2010, **14**, 38–48.
- 66 V. Kalra, F. Escobedo and Y. L. Joo, *J. Chem. Phys.*, 2010, **132**, 24901.
- 67 A. Tuteja, M. E. Mackay, S. Narayanan, S. Asokan and M. S. Wong, *Nano Lett.*, 2007, **7**, 1276–1281.
- 68 A. Tuteja, P. M. Duxbury and M. E. Mackay, *Macromolecules*, 2007, **40**, 9427–9434.
- 69 A. M. Mathai, P. Moschopoulos and G. Pederzoli, *Rend. del Circ. Mat. di Palermo*, 1999, **48**, 163–190.
- 70 J. W. Eaton, D. Bateman, S. Hauberg and R. Wehbring, *GNU Octave version 4.4.0 manual: A high-level interactive language for numerical computations*, 2018.
- 71 W. Nowicki, *Macromolecules*, 2002, **35**, 1424–1436.
- 72 S. K. Kumar, N. Jouault, B. Benicewicz and T. Neely, *Macromolecules*, 2013, **46**, 3199–3214.
- 73 C. M. Hansen, *Hansen Solubility Parameters: A User's Handbook, Second Edition*, CRC Press, 2007, vol. 2.
- 74 E. Stefanis, I. Tsivintzelis and C. Panayiotou, *Fluid Phase Equilib.*, 2006, **240**, 144–154.
- 75 G. P. Van der Beek, M. A. C. Stuart, G. J. Fleer and J. E. Hofman, *Macromolecules*, 1991, **24**, 6600–6611.
- 76 P. Hudon, I.-H. Jung and D. R. Baker, *Phys. Earth Planet. Inter.*, 2002, **130**, 159–174.
- 77 Y. He, C. Cao, Y.-X. Wan and H.-P. Cheng, *J. Chem. Phys.*, 2006, **124**, 024722.
- 78 M. J. Marmo, M. A. Mostafa, H. Jinnai, F. M. Fowkes and J. A. Manson, *Ind. Eng. Chem. Prod. Res. Dev.*, 1976, **15**, 206–211.
- 79 F. M. Fowkes and M. A. Mostafa, *Ind. Eng. Chem. Prod. Res. Dev.*, 1978, **17**, 3–7.
- 80 F. M. Fowkes, *Rubber Chem. Technol.*, 1984, **57**, 328–343.
- 81 D. L. Allara, F. M. Fowkes, J. Noolandi, G. W. Rubloff and M. V. Tirrell, *Mater. Sci. Eng.*, 1986, **83**, 213–226.
- 82 F. M. Fowkes, *J. Adhes. Sci. Technol.*, 1990, **4**, 669–691.
- 83 R. S. Drago, G. C. Vogel and T. E. Needham, *J. Am. Chem. Soc.*, 1971, **93**, 6014–6026.
- 84 J. Liu, Y. Wu, J. Shen, Y. Gao, L. Zhang and D. Cao, *Phys. Chem. Chem. Phys.*, 2011, **13**, 13058.
- 85 C. Vander Linden and R. Van Leemput, *J. Colloid Interface Sci.*, 1978, **67**, 63–69.
- 86 G. Wu, S. Asai, M. Sumita and H. Yui, *Macromolecules*, 2002, **35**, 945–951.
- 87 T. Hamieh, *Soft Mater.*, 2010, **9**, 15–31.
- 88 Q. Huang, O. Mednova, H. K. Rasmussen, N. J. Alvarez, A. L. Skov, K. Almdal and O. Hassager, *Macromolecules*, 2013, **46**, 5026–5035.
- 89 L. J. Fetters, D. J. Lohse and R. H. Colby, in *Physical Properties of Polymers Handbook*, Springer New York, New York, NY, 2007, pp. 447–454.
- 90 W. Lu, P. Yin, M. Osa, W. Wang, N.-G. Kang, K. Hong and J. W. Mays, *J. Polym. Sci. Part B Polym. Phys.*, 2017, **55**, 1526–1531.

9. Author's CV

Education

2018 Ph.D. – Advanced materials at Brno University of Technology, CEITEC

2014 Master degree – Chemistry, technology and properties of materials, Brno University of Technology, Faculty of Chemistry

Publication highlights

1. Lepcio, P.; Ondreas, F.; Zarybnicka, K.; Zboncak, M.; Caha, O.; Jancar, J. Bulk polymer nanocomposites with preparation protocol governed nanostructure: the origin and properties of aggregates and polymer bound clusters. *Soft Matter*. 2018, **14**, 2094-2103. ISSN: 1744-6848.
2. Lepcio, P.; Ondreas, F.; Jancar, J. The effect of nanoparticles on rheological behavior of polystyrene solutions under large amplitude oscillation shear (LAOS). *Material Science Forum*. 2016, **851**, pp 215–220. ISSN: 0255-5476.
3. V. Cech, A. Knob, H. A. Hosein, A. Babik, P. Lepcio, F. Ondreas and L. T. Drzal, Enhanced interfacial adhesion of glass fibers by tetravinylsilane plasma modification, *Compos. Part A Appl. Sci. Manuf.*, 2014, **58**, 84–89.

Conferences

1. 17th International Conference on Deformation, Yield and Fracture of Polymers, Rolduc, NL, 2018, 1st prize award for best poster.
2. Workshop on Structure and Dynamics of Polymer Nanocomposites, Montpellier, France, 2015.
3. XV. mezioborové setkání mladých biologů, biochemiků a chemiků 2015, Milovy, 2015.
4. Chemistry & Life 2015, Brno, 2015.
5. Curie – Pasteur – CEITEC joint young scientist retreat, Brno, 2017.

Internships

1. In Natural Materials Group at The University of Sheffield supervised by Dr. Chris Holland, Sheffield, UK, January–June 2016.

Project participation

1. Recycling of waste polycarbonates and development of advanced polycarbonate thermoplastic blends for primary production applications, TJ01000320, 2018-2019.
2. Mechanisms and kinetics of NP self-assembly in hierarchical polymer composites, GA15-18495S, 2015-2017.
3. Vliv kinetických a termodynamických podmínek přípravy na disperzní stavy polymerních nanokompozitů a jejich termomechanické vlastnosti, STI-J-15-2856, 2015.
4. Řízení samo-uspořádání nanočástic v polymerních kapalinách a vliv vzniklé nanostruktury na termomechanické vlastnosti výsledných nanokompozitů, STI-J-16-3650, 2016.
5. Mechanické vlastnosti polymerních nanokompozitů s řízenou strukturou, STI-J-17-4204, 2017.

Fields of interest

- Polymers, composites and nanocomposites, self-assembly, rheology, thermomechanics, recycling, waste management, 3D printing

Techniques and skills

- Research design, laboratory work, sample preparation, data evaluation and interpretation, results presentation to scientific audience, preparation and submission of research papers and project proposals

- Operator of: rheology, FTIR, DSC, TGA, DLS, CLSM, AFM
- Computer command: office suite, OriginLab, programming and scripting (Object Pascal, Matlab, Arduino), 2D and 3D graphics
- English C1–C2

10. Abstract

Polymer nanocomposites (PNCs) hold a great promise as future lightweight functional materials processable by additive manufacturing technologies. However, their rapid deployment is hindered by their performance depending strongly on the nanoparticle (NP) spatial organization. Therefore, the ability to control the nanoparticle dispersion in the process of PNCs preparation is a crucial prerequisite for utilizing their potential in functional composites. This work investigates solution blending of PNCs in a model glass forming polymer matrix, a bulk processing technique of a tailored NP spatial organization controlled by structural and kinetic variables of the preparation protocol. The presented results describe the differences between nanoparticle induced changes on the rheological behavior of a polystyrene solution under large amplitude oscillation shear (LAOS). High-affinity OP-POSS NPs seem to interact with the PS at low filler loadings and form stiffened aggregates, whereas low-affinity OM-POSS NPs remained rather uninvolved in the polymer deformation at these conditions. Furthermore, an interest was focused on the impact of the blending solvent on the NP spatial arrangement in silica/PMMA and silica/PS nanocomposites, which has already been suggested as the controlling parameter of the solid-state structure. An emphasis was put on the qualitative differences between “poorly dispersed” NP arrays which, by combination of rheological assessment and structural analysis (TEM, SAXS), were identified as chain bound clusters and two types of aggregates, one of thermodynamic and the other of a kinetic origin, which are characterized by substantially distinct formation kinetics and mismatched properties compared to individually dispersed NPs and each other. The currently observed types of NP dispersion were quantitatively linked with their rheological properties during the solution blending step and the amount of polymer adsorption and depletion attraction. The results were compared to the PRISM theory. Finally, the importance of NP spatial organization was demonstrated on the comparison of glass transition temperatures of various structures at constant chemical composition.